Published August 31, 2009

with the expected responses to stepwise changes in temperature, and suggest that the cellular temperature under whole cell recordings changed rapidly.

During a temperature pulse, the temperature sensed by the channel molecule in situ was evaluated. Because the gating of proton channels exhibits a high sensitivity to temperature (Byerly and Suen, 1989; Kuno et al., 1997; DeCoursey and Cherny, 1998), the accelerated gating kinetics upon heating pulses were used for the evaluation. First, the activation time courses of proton currents at a steady-state bath temperature, elicited by depolarizing pulses to 0 mV, were fitted with a triple-exponential function, and the time constants were plotted as a function of temperatures measured in the vicinity of the cell (Fig. 5, filled symbols). Then, the warming temperature pulses were applied during the gating activation. When the temperature pulses were applied after faster activation components were nearly completed, the accelerated time courses for the residual activation during temperature pulses were fitted by a single-exponential function. These time constants (Fig. 5, open symbols) were superimposed on the plot of time constants observed at the steady-state bath temperature. The data points from the temperature pulses overlapped onto the distribution of the slowest components of the activation time constants. The Q_{10} for the activation time constant measured under the pulse method was similar to that measured when the entire bath was temperature controlled (5.6 ± 0.5; $n = 33$). These data indicate that the temperatures applied to the channel molecules on the cell were monitored successfully by the thermocouple adjacent to the cell.

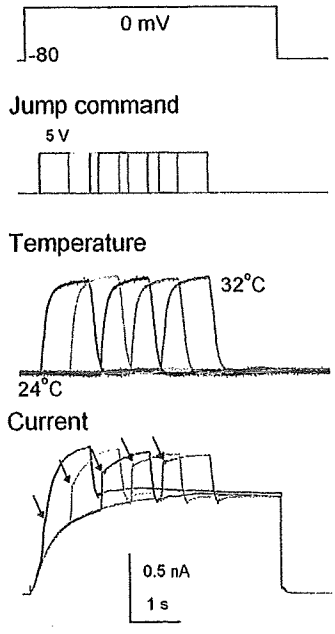

Figure 4. Current responses to temperature pulses. A patch-clamped cell at an intracellular pH of 5.5 was placed in the midst of a laminar outflow, and an ultrafine thermocouple was located downstream of the cell within 15 μm. Proton currents were elicited by depolarizing pulses to 0 mV (top; pulse duration was 4 s), during which a temperature pulse of 1 s (from 24 to 32°C; ΔT = 8°C) was applied at different phases of the gating activation. The pulse command indicates the driving voltages to the piezoelectric device. The thermocouple signals displayed reproducible changes for the repetitive temperature pulses. Ensemble current traces with responses to temperature pulses elicited at different timings of the activation are superimposed.

Temperature pulse experiments under various conditions

Temperature pulses applied during the steady state of gating activation produced clear stepwise changes in the currents upon both the onset and termination of the pulses (Fig. 6 A). Upon the return to the prepulse temperature, the amplitudes of the currents reverted to those before the pulse, confirming that the open-state probability had not been changed during a pulse. Pulses with various magnitudes of ΔT either warming or cooling were applied at various temperatures (pre-jump temperature; Fig. 6 A, a, c, and f, and b, d, and e). At low temperatures (Fig. 6 A, e and f), long (>8 s) depolarization pulses were required for the gating activation to reach the steady state. At −100 mV, which is outside of the activation range for the gating, temperature jumps produced negligible changes in current amplitude (Fig. 6 B).

The ratio of current amplitudes, I_{ratio}, as an index for temperature dependence

To evaluate the temperature dependence of current amplitudes immediately before and after a temperature

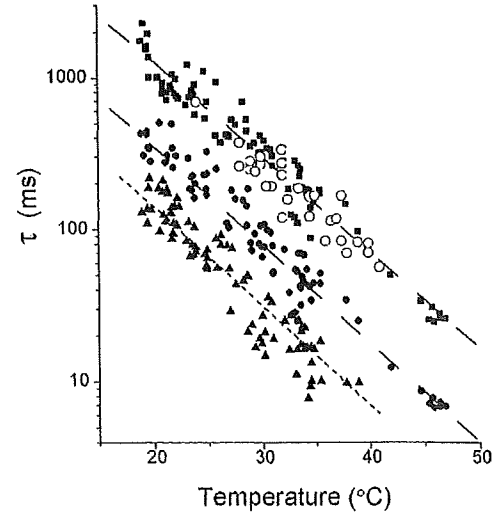

Figure 5. Temperature-dependent time constants for the activation gating. The activating currents at 0 mV were fitted by a triple-exponential function. Temperature pulses were applied after the faster activation phases were nearly completed. Current traces during temperature pulses were fitted with a single exponential. Three time constants at various temperatures (filled symbols) and the time constant during the pulse (open symbols) are shown. The data were obtained from a single cell.

Published August 31, 2009

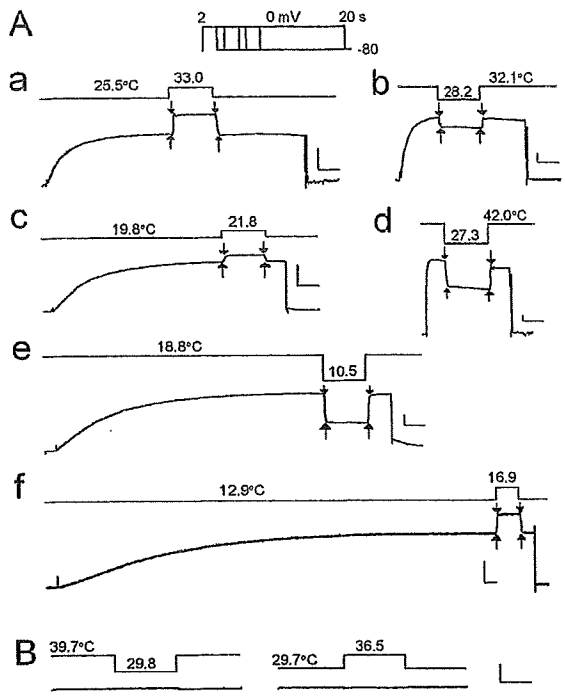

Figure 6. Responses of the proton currents to temperature pulses (pH_i/pH_o, 5.5/7.3). (A) Proton currents were elicited by depolarizing steps to 0 mV (inset; the voltage command with the holding potential of −80 mV). Temperature pulses (blue lines; duration, 1 s) were applied during the steady state of the gating activation. Current amplitudes were measured immediately before and after the onset (red arrows) and termination (blue arrows) of the pulses. The depolarizing pulses were followed by hyperpolarizing ramps (20 ms), and the outward tail currents were not obvious in these traces. (B) Temperature pulses were applied at the hyperpolarizing potential of −100 mV.

jump, the current amplitudes for each jump were plotted as a function of pre-jump and jump temperatures, and the points were connected to draw a vector (jump vector; Fig. 7 A). The direction of the vectors indicates whether the pulse was cooling (down) or warming (up). Plots of the vectors from six different cells over a wide range of temperatures with variably sized ΔTs and directions (warming or cooling) showed a general trend of vector flow.

Jump vectors were examined for different membrane potentials (Fig. 7 B). Temperature jumps of a fixed ΔT (from 16.7 to 12.7°C) were applied during variable depolarizing steps. Each column of arrows represents jump vectors from a cell. The slopes of the vectors on the logarithmic scale were almost identical, even though the current amplitudes at different membrane potentials differed considerably.

The ratios of the current amplitudes were calculated from the vectors (current ratio; $I_{ratio} = I_{jump}/I_{pre\text{-}jump}$) and were plotted at different membrane potentials (Fig. 7 C), where the ΔTs were set differently for cells. The I_{ratio}s were distributed nearly horizontally, indicating that the I_{ratio} was not affected by the current amplitudes.

Temperature dependence of Q_{10} over a wide temperature range

A plot of the values of I_{ratio}s as a function of ΔTs shows nearly linear relationships. I_{ratio}s were measured from many cells over a wide range of pre-jump temperatures (4–49°C) and ΔTs (±15°C) (see three-dimensional plot in Fig. S2). I_{ratio}–ΔT relationships are shown for different ranges of pre-jump temperatures (Fig. 8). Linear relationships hold at relatively narrow ranges of pre-jump

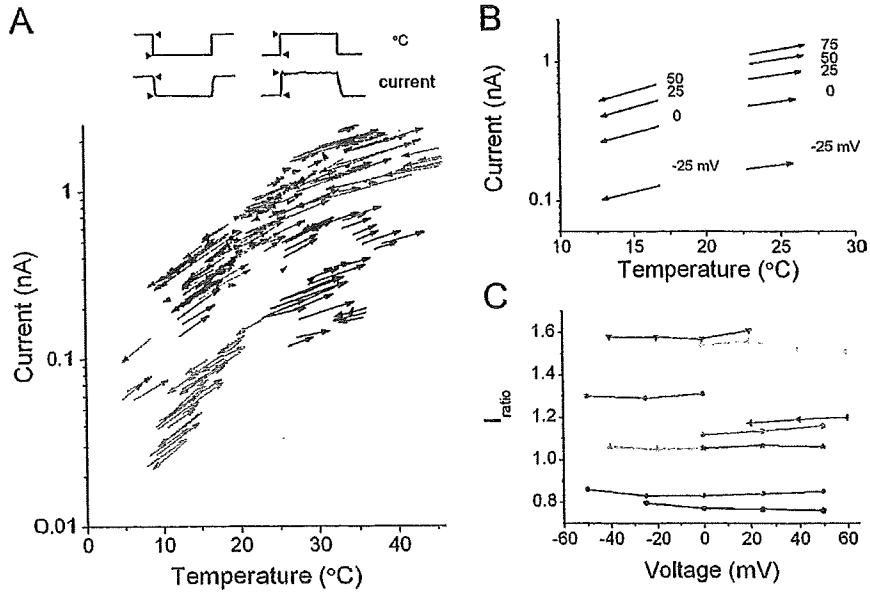

Figure 7. The jump vector plot and current ratios. (A) The jump vector plot over a wide temperature range (pH_i/pH_o, 5.5/7.3). Current amplitudes immediately before and after a temperature jump (arrow heads) were plotted for pre-jump (tail of arrows) and jump (head of arrows) temperatures. Arrows were obtained from six different cells. Each colored arrow represents data from a single cell. A depolarization pulse of 0 mV was applied. Note that the axis for the current amplitude is logarithmic. (B) The jump vector plots at different membrane potentials ranging from −25 to +75 mV. Arrows from different membrane potentials in two different cells (left column, cool-down jump; right column, heat-up jump) are shown. (C) I_{ratio}s at different membrane potentials. A set of I_{ratio}s from nine cells is shown. For each cell ΔT was fixed.

Published August 31, 2009

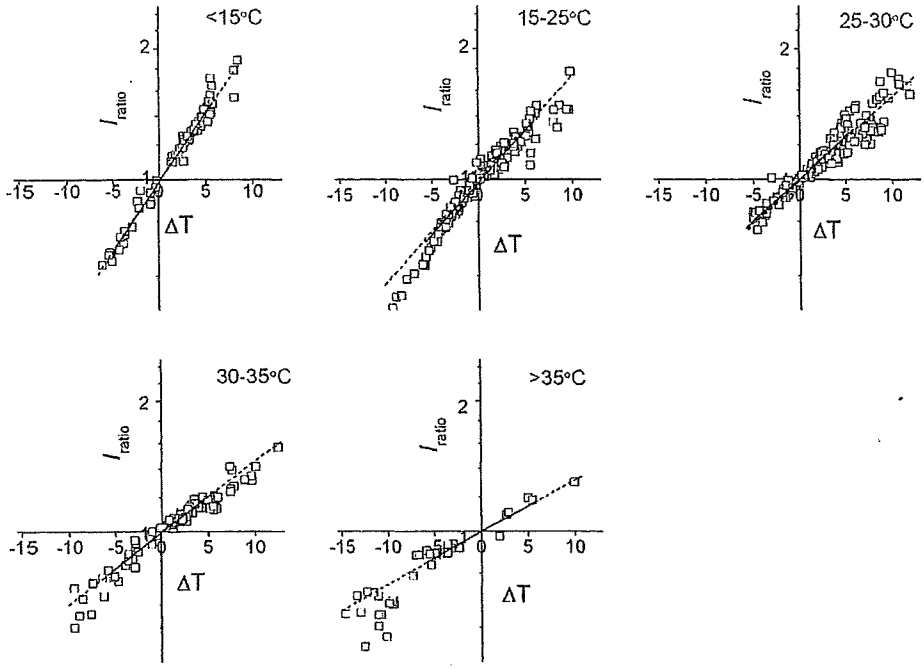

Figure 8. Temperature dependencies of I_{ratio}s. I_{ratio} as a function of ΔT for different pre-jump temperatures. The data points were fitted by a linear function, and the Q_{10} values were obtained from the slopes. Solid lines were fitted to the data with the absolute ΔT value <5°, and the broken lines are the extrapolations. Q_{10} values were 1.98 < 15°C, 1.79 for 15 ≤ T < 25°C, 1.60 for 25 ≤ T < 30°C, 1.46 for 30 ≤ T < 35°C, and 1.32 > 35°C.

temperatures. The slope is a measure of temperature dependence of proton currents, and the Q_{10} value was calculated (see Materials and methods). Fig. 8 demonstrates that the Q_{10} value decreased significantly over a measured temperature range. A similar relation was observed at pH 6.2 (not depicted).

To obtain thermodynamic clues for this phenomenon, the jump vector data were expressed as an Arrhenius plot, in which pairs of current amplitudes for each temperature jump were plotted against $1/T$ (T, the absolute temperature; Fig. 9). The slopes of the arrows became steeper as the temperature was decreased (toward the right of the horizontal axis) and, overall, the arrows indicate a trend that is curved (convex). A curved Arrhenius plot is generally considered to indicate the presence of multiple processes with different underlying natures (Gutfreund, 1995; Fersht, 1999).

To quantify the temperature dependence, the mean Q_{10} values were plotted as a function of temperature (Fig. 10). The Q_{10} value of 2.2 at 10°C decreased monotonically as the temperature was increased and reached 1.3 at 40°C. The strong temperature dependence of the Q_{10} values has not been reported in earlier studies, at least for the permeation of channels.

The rate theory (Kramers, 1940) was applied to express proton permeation at different temperatures with thermodynamic parameters (see Eq. A1). Q_{10} as a function of T can be expressed as

$$Q_{10}(T) = Exp\left[10\left(\frac{\Delta H^{\ddagger}}{RT^2} + \frac{1}{T}\right)\right], \quad (2)$$

where $\Delta H^{\ddagger}$ represents the activation enthalpy. This equation demonstrates that Q_{10} value changes at different temperatures, the extent of which can be estimated. The changes of Q_{10} at constant $\Delta H^{\ddagger}$ values are shown in Fig. 10 (dotted lines, iso-enthalpy lines). As expected, the experimentally obtained Q_{10}s did not align on the

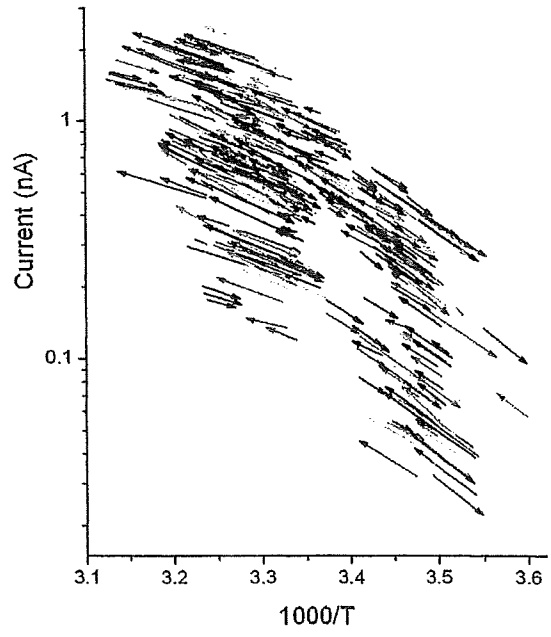

Figure 9. An Arrhenius plot for the proton permeation process through the voltage-gated proton channel. Each arrow represents data for the onset of a temperature pulse.

Published August 31, 2009

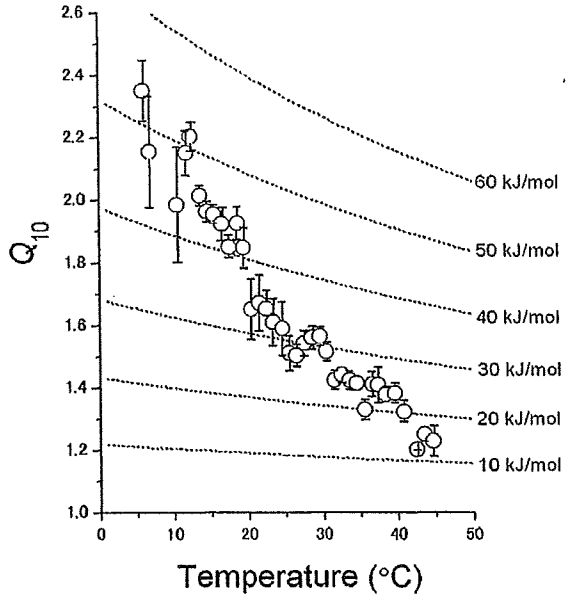

Figure 10. Temperature dependence of Q_{10} values. Q_{10} values were calculated from the data of temperature jump experiments. A set of dotted lines indicates temperature-dependent Q_{10} values for fixed activation enthalpy (iso-enthalpy line).

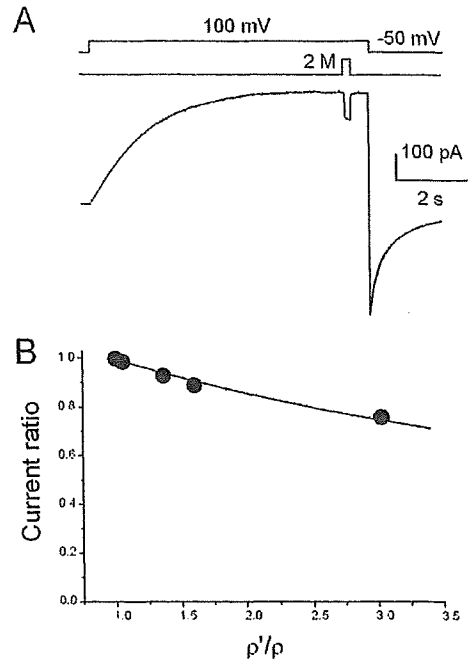

Figure 11. Estimation of the access resistance. (A) Current traces for the resistivity pulse experiments. The pHs were symmetrical (pH, 5.5), and the temperature was 23°C. A patch-clamped cell was exposed briefly to a solution containing 2 M sorbitol. The current amplitudes were measured immediately before and after a jump. (B) Current ratios as a function of the relative resistivity of the solutions. ρ is the resistivity of the bathing solution, and ρ' is the resistivity of the pulse solution. The data were fitted by Eq. A10. The ratio of the resistances (R_{AR}/R_{Ch}) was 0.25.

iso-enthalpy lines, but cut across them. What is the underlying mechanism for the strong temperature dependence of Q_{10}? Multiple processes with different thermodynamic natures are involved in the measured currents. From the theoretical prediction, one possible candidate underlying the observations is the access resistance that develops instantaneously ($<10^{-10}$ s; see Experimental strategy and Appendix), and hence its contribution to the measured current even with the rapid temperature change cannot be eliminated.

Estimation of the access resistance

Direct measurements of the access resistance (R_{AR}) are impossible, but the relative contribution of R_{AR} to the measured current (or R_{total}) can be estimated. Hall's equation indicates that R_{AR} changes with the resistivity of the bathing solution (see Eq. A7). Therefore, if a cell is perfused with a different resistivity solution, changes in the external R_{AR} lead to changes in R_{total}. Analyses of an equivalent electrical circuit having R_{Ch} (the channel resistance) and R_{AR} in series (see Appendix) demonstrated that the ratio of R_{total} in two different resistivity solutions gives the ratio of R_{AR} and R_{Ch} (see Eq. A8). Here, an experimental method for evaluating R_{AR}/R_{Ch} was developed (the resistivity pulse method [R pulse method]). Proton currents were elicited by depolarization pulses to +100 mV. After reaching steady-state activation, the cells were exposed to the high resistivity solution for a short period of time (250 ms; Fig. 11 A; see Materials and methods) (Ando et al., 2005), and current amplitudes before and after a resistivity jump were measured. In these experiments, solutions on both sides of the membrane were set symmetrically (pH, 5.5); hence, R_{AR}s on the intracellular and extracellular sides were assumed to be identical.

The current trace demonstrated, surprisingly, large decreases in amplitudes upon exposure to a high resistivity solution, suggesting a large contribution of the access resistance. The current ratios were plotted as a function of the relative resistivities of the solutions (Fig. 11 B). Proton currents decreased gradually as the resistivity of the external solution was increased. The R_{Ch}/R_{AR}s were obtained through fitting the current ratio of Eq. A11 to the data. The value of R_{Ch}/R_{AR} was 3.8 and that of R_{Ch}/R_{total} was 0.66 at 23°C. A notable contribution of R_{AR} to R_{total} suggests that the observed Q_{10} values do not solely represent temperature dependence of the channel per se, but represent a weighted average for those of the channel and the access resistance. Therefore, we redefine here the observed Q_{10} as the apparent Q_{10} (Q_{10}^{app}). It should be noted that R_{Ch}/R_{AR} is not constant over the temperature range because the temperature dependencies of the channel and access resistances differ. Then it is likely that the strong temperature dependence of Q_{10}^{app} is produced by the relative contribution of Q_{10} for the

Published August 31, 2009

access resistance (Q_{10}^{AR}) and for the channel (Q_{10}^{Ch}), which varies as the temperature changes.

The Q_{10}^{Ch} was decomposed from Q_{10}^{app} by the series resistance model (see Appendix). Each resistance (R_{Ch} and R_{AR}) can be characterized by its own thermodynamic parameters, such as the activation enthalpy and entropy. An equation was derived for the temperature dependence of the Q_{10}^{app} values as a function of the thermodynamic parameters for the channel and access resistance (see Eq. A14). In this equation, temperature dependence of R_{AR} (Q_{10}^{AR}) can be represented by of the buffer solution (Hall's equation) (Hall, 1975), which was evaluated by measuring the conductivity of the buffered solution at different temperatures (Fig. 12 A). The Q_{10}^{AR} value was 1.2 at 25°C and decreased slightly at higher temperatures (Fig. 12 B). If the thermodynamic parameters for the channel, in addition to the access resistance, would be given, the series resistance model would provide temperature dependencies of observable currents and Q_{10}^{app}.

Conversely, now that data for temperature dependency of Q_{10}^{app} and the thermodynamic parameters of the access resistance are available (data points in Fig. 12 B), thermodynamic parameters for the channel were obtained through optimizing the parameter as to fit the calculated Q_{10}^{app} line to the Q_{10}^{app} data. The blue line in Fig. 12 shows the estimate for the temperature dependence of Q_{10}^{Ch} (an iso-enthalpy line). In this figure, strong temperature dependence of Q_{10}^{app} was decomposed into Q_{10}^{AR} and Q_{10}^{Ch}. Finally, the activation enthalpy ($\Delta H^{\ddagger}$) for proton permeation through the channel per se was determined to be 64 kJ/mol. (Similar values of thermodynamic parameters for the channel [or Q_{10}^{Ch}] were obtained through fitting procedures using data of I_{ratio}s at different temperatures and ΔTs; Fig. S2).

DISCUSSION

The temperature dependencies of proton permeation through the voltage-gated proton channel per se (Q_{10}^{Ch}) are masked by many layers of phenomena, and the aim of this study was to isolate Q_{10}^{Ch}. By applying temperature pulse methods, the overlying factors, such as the changes in the number of active channels and the driving forces of proton permeation, were successfully excluded. The measured Q_{10}, however, exhibited unexpectedly high temperature dependence, which cannot be accounted for by a simple physical process (hence named Q_{10}^{app}). We suspected that Q_{10}^{app} represents a mixture of multiple processes with different temperature dependencies. The novel resistivity pulse experiments allowed the quantitative evaluation of the access resistance (R_{AR}) and revealed significant contribution of R_{AR}. Finally, we extracted Q_{10}^{Ch}, attained for the first time, and the value was 2.5 at room temperature and the activation enthalpy was 64 kJ/mol. These thermodynamic features will be discussed for the underlying mechanisms of proton permeation through the voltage-gated proton channel.

Verification of the temperature pulse method

The T pulse method is characterized by its rapid change of temperature, which minimizes the contributions of the slowly developing events, i.e., proton depletion and concentration polarization. The validity of the T pulse method was demonstrated in various ways, as follows. The stepwise changes in temperature were confirmed by the rectangular shapes of the measured liquid junction potentials (Fig. 1 B) and of the proton currents themselves (Figs. 8–10). Throughout the experiment, the temperature in the vicinity of the cell was monitored

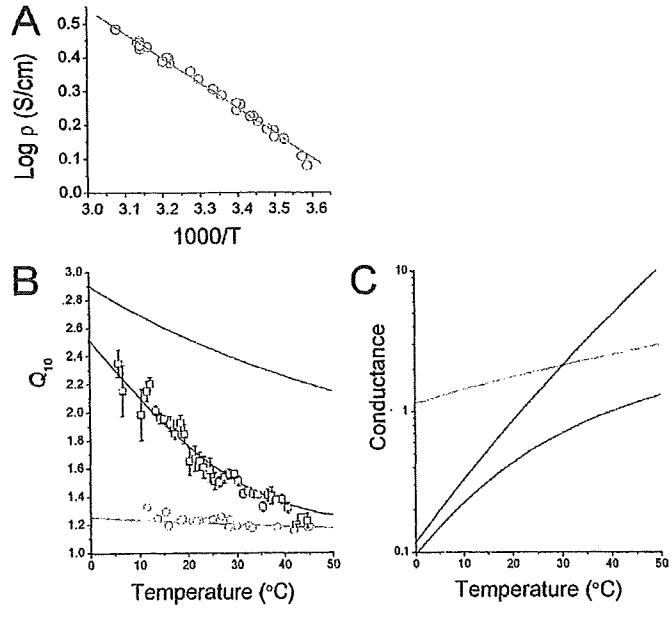

Figure 12. Decomposition of apparent Q_{10} (Q_{10}^{app}). (A) Measured conductance (ρ) for the Mes-buffered solution represented as the Arrhenius plot. The $\Delta H^{\ddagger}$ value was 14.0 kJ/mol, and the preexponential factor was 556.7. (B) Temperature dependencies of Q_{10}^{AR} (green symbols and line), Q_{10}^{Ch} (blue), and Q_{10}^{app} (red symbols and line) values. Q_{10}^{AR}s were calculated from the data for A (see Materials and methods). A $\Delta H^{\ddagger}$ value of 12.5 kJ/mol was obtained by fitting to the Q_{10}^{AR} values. $\Delta S^{\ddagger}$ was set to zero. Using $\Delta H^{\ddagger}$ and $\Delta S^{\ddagger}$ values for the access resistance, the values of $\Delta H^{\ddagger}$ and $\Delta S^{\ddagger}$ for the channel were estimated through fitting Eq. A10 to Q_{10}^{app} data. $\Delta H^{\ddagger}$, $\Delta S^{\ddagger}$, and ω_C for the channel were 63.7 kJ/mol, 8.49 J/mol/T, and 0.0115. Q_{10}^{Ch} (blue line) was drawn using the above fitted parameters. (C) Temperature dependencies of conductances for access resistance (green), channel (blue), and total (red) values. Conductances were calculated using the thermodynamic parameters.

Published August 31, 2009

with an ultrafine thermocouple (Fig. 1), which demonstrated that ambient temperature of the channels in situ (on the plasma membrane) was well controlled by the pulse method (see Fig. 7). These results indicate that the temperature pulse method readily provides variable up-and-down temperature jumps to whole cell clamped cells within a few milliseconds in a reproducible and accurate manner.

The I_{ratio} introduced here as a robust measure of temperature dependence served for calculating Q_{10}^{app}. Q_{10}^{app}s were evaluated under various experimental conditions: at different intracellular pHs, at different membrane potentials (Fig. 7), and in the presence and absence of droop.

Q_{10} for proton permeation per se extracted from the temperature-dependent Q_{10}^{app}

A key finding of the present study was that the Q_{10}^{app} values changed significantly over a wide temperature range (Fig. 10). Generally, the Q_{10} value should change somewhat. In fact, simple physical processes, such as proton-transfer processes through the access region and the channel pore, can be described by the rate theory (see Eq. A1), and the temperature dependence of the pre-exponential factor for the rate equation leads to slight temperature dependence of Q_{10}, which follows the isoenthalpy line (Fig. 10). The large changes in the Q_{10}^{app} values over ~1 unit between 4 and 49°C suggest that multiple processes with different temperature dependences are involved.

A seminal paper by Decker and Levitt (1988) led us to examine the contribution of access resistance to the total proton current in the presence of a high concentration buffer. The *R* pulse method revealed unexpectedly large changes in current amplitudes upon exposure to the high resistivity solution, suggesting a significant contribution of the access resistance to the measured current. A simple model for resistances in series of the channel and access regions (the series resistance model) was adopted for quantitative evaluation, and the R_{Ch}/R_{total} ratio was estimated to be 0.66 at room temperature. This value makes evident that the contribution of the access resistance to the measured current was important.

The series resistance model demonstrates that if thermodynamic parameters for the channel and the access region are given, the temperature-dependent Q_{10}^{app} can be readily calculated. The thermodynamic parameters for the access resistance were estimated from that of the resistivity of the buffered solution (Fig. 12 B, green line) (Hall, 1975). Now that Q_{10}^{app} and Q_{10}^{AR} are given, Q_{10}^{Ch} and its thermodynamic parameters can be estimated through the fitting procedure.

Fig. 12 B demonstrates graphically how the strong temperature dependency of Q_{10}^{app} is decomposed into Q_{10}^{Ch} and Q_{10}^{AR}. At low temperature the Q_{10}^{Ch} predominates, and at high temperature the Q_{10}^{AR} predominates. Q_{10}^{app} traverses from Q_{10}^{Ch} to Q_{10}^{AR} through the measured temperature range. The activation enthalpy for proton permeation through the channel was finally extracted. (These thermodynamic parameters were also obtained from direct fit to the I_{ratio} data; Fig. S2.) The Q_{10}^{Ch} value was 2.5 at room temperature, and the $\Delta H^{\ddagger}$ value was 64 kJ/mol.

Before discussing the implication of the activation enthalpy for the proton permeation, the physiological relevance of Q_{10}^{app} will be discussed.

The Q_{10}^{app} under physiological conditions

The Q_{10}^{app} values obtained here were smaller than the Q_{10} of earlier reports (5.3 ≤ 20°C and 2.8 > 20°C) (DeCoursey and Cherny, 1998), which might be overestimates because they included the contribution of changes in the numbers of activatable channels at different temperatures (Fig. S3). In Fig. 12 C, the temperature-dependent conductance was decomposed into the conductance for the channel (blue line) and that for the access resistance (green line). This figure was drawn using the thermodynamic parameters, demonstrating the relative contributions. The temperature-dependent conductances of the channel and the access resistance form asymptotes for the observed conductance (Fig. 12 C, red line). These parameters gave the ratio R_{Ch}/R_{total} as 0.46 at 23°C, which is in rough agreement with the ratio predicted from the *R* pulse method. Because the temperature dependence of the channel conductance is much higher than that of access resistance, the channel conductance overwhelmed that of the access resistance and the whole process became diffusion limited above the crossing point of ~30°C. In physiological conditions, in which the buffer concentrations are much lower than in the present experimental conditions, the temperature dependence of the voltage-gated proton channel, Q_{10}^{app}, is apparently governed by diffusion-limited processes and is almost indistinguishable from those of other types of ion channels.

Mechanisms for proton-selective permeation

The temperature dependence of proton permeation has been studied systematically only for the gramicidin A (gA) channel, which is proton conducting, but not proton selective (Andersen, 1984; Heinemann and Sigworth, 1989; Oiki et al., 1995; Koeppe and Anderson, 1996). Over a wide temperature range (Chernyshev and Cukierman, 2002), the Q_{10} values were nearly constant (Cukierman, 2000) and the $\Delta H^{\ddagger}$ values for proton permeation through most gA channels were 10–20 kJ/mol (Bamberg and Läuger, 1974; Akeson and Deamer, 1991; Chernyshev and Cukierman, 2002). These values are similar to those for proton diffusion in an aqueous solution, in which the Grotthuss mechanism predominates (Eigen, 1964; Agmon, 1995; Day et al., 2000; Limbach et al., 2006), and are in general agreement with the activation enthalpy for the buffered diffusion (Fig. 12 A). However,

Published August 31, 2009

it has been reported that the contribution of the access resistance to the recorded single-channel current is significant for proton permeation through the gA channel (Decker and Levitt, 1988; Cukierman, 2000; Schumaker et al., 2000; Schumaker, 2003; Braun-Sand et al., 2005). Therefore, the measured temperature dependence of earlier studies for the gA channel may be governed largely by the access resistance, similar to the voltage-gated proton channel. In fact, breaks in linearity or curved Arrhenius plots have been reported for gA channels (Chernyshev and Cukierman, 2002). The lower Q_{10} may represent the diffusion-limited ion access, and the higher Q_{10} (>30 kJ/mol) could represent the inherent proton permeation process.

The voltage-gated proton channel exhibits nearly perfect proton selectivity compared with the gA channels. We estimated the activation enthalpy of proton permeation through the channel to be 64 kJ/mol. This is essentially the first quantitative evaluation of a thermodynamic parameter for proton permeation through proton-selective channels. What is the underlying mechanism of the $\Delta H^{\ddagger}$ value for the proton permeation? Quantitative comparison of the present $\Delta H^{\ddagger}$ value with those of other types of channels must be reserved until the genuine $\Delta H^{\ddagger}$ values without effect of the access resistance would become available for other types of channels. Still, we anticipate that $\Delta H^{\ddagger}$ for the proton channel is significantly higher than for the gA channel, and a gap between the $\Delta H^{\ddagger}$ value of the proton channel and gA channels cannot be accounted for by simple modifications of the proton jump mechanism through a single-file pore. We present here a hypothetical mechanism for proton-selective permeation: A proton-selective site(s) should exist along a water-filled pore, and its configuration needs to be rearranged upon proton transfer, which would account for the additional cost of $\Delta H^{\ddagger}$ for the proton permeation. The mechanism of proton permeation through the molecular candidate of the voltage-gated proton channels (Ramsey et al., 2006; Sasaki et al., 2006; DeCoursey, 2008) and other proton-selective pores in the voltage sensor domain of potassium channels (Starace and Bezanilla, 2004) has not been studied. However, given the structural elements that the candidates possess, such as water crevices toward protonation sites, our hypothetical mechanism is compatible with those that the candidates may exhibit. Involvement of local structural changes during rearrangement of proton-accepting histidine residues may account for the observed activation enthalpy. Those are thermodynamic aspects of experimental evidence supporting the candidate molecule as the molecular entity of the voltage-gated proton channel.

Here, we conclude the temperature dependence of the voltage-gated proton channel. Q_{10}^{app} is a measure that represents the overall nature of proton permeation, including the access resistance. The value characterizes apparent behavior of the proton channel under physiological conditions and is almost indistinguishable from that for other types of channels (Hoffmann and Dionne, 1983; Urry et al., 1984; Grygorczyk, 1987; Miller et al., 1988; Sitsapesan et al., 1991; Milburn et al., 1995; Hille, 2001; Chernyshev and Cukierman, 2002). On the other hand, Q_{10}^{Ch} is a measure to characterize the proton permeation in the channel per se, and we have proposed an underlying mechanism of proton-selective permeation. These thermodynamic clues are prerequisite to advance our understanding of the mechanism of action for proton-selective permeation.

APPENDIX

Local proton concentration

In the presence of buffer, the concentration polarization is confined to a limited space, which otherwise extends farther from the membrane. Zifarelli et al. (2008) simulated the concentration profile of protons near the membrane. Their numerical evaluation showed that if the flux of protons is constant, the concentration polarization develops relatively slowly over a time range of several tens to hundreds of milliseconds. For example, the pH at the outer vicinity of the membrane decreased by 1.3 U in the presence of buffer concentration as low as 0.1 mM after 5 s of a proton efflux of 500 pA. This local proton accumulation decreased to a ΔpH of 0.07 U when the buffer concentration was increased to 2 mM. Following the reported method, we simulated the local accumulation when the buffer concentration was increased to 100 mM (our experimental condition). The ΔpH was only 0.0013 U at the vicinity of the membrane. The time course of the development was fitted by a double-exponential function, and the smaller time constant was ~60 ms. The slow development and attenuation of the concentration polarization in the concentrated buffer were used in the experimental strategy.

Temperature-dependent Q_{10}

The rate constant for the proton permeation was expressed in Kramers' theory (Kramers, 1940; Hänggi et al., 1990; Berry et al., 2000):

$$k(T) = \frac{\omega_A \omega_C}{2\pi\zeta} Exp\left[-\frac{\Delta H^{\ddagger} - T\Delta S^{\ddagger}}{RT}\right], \quad \text{(A1)}$$

where the preexponential factor can be expressed as:

$$\frac{\omega_A \omega_C}{2\pi\zeta} = \frac{\omega_C}{\zeta}\frac{\omega_A}{2\pi} = \frac{\omega_C}{\zeta}\frac{k_B T}{h}. \quad \text{(A2)}$$

In these equations, ζ is the friction coefficient, ω_C is the characteristic frequency, h is the Planck constant, R is the gas constant, and k_B is the Boltzmann constant.

Published August 31, 2009

This equation for condensed systems is valid in the limit of large friction. The temperature dependence for the friction coefficient is:

$$\zeta(T) = \frac{1}{aExp[-b/T]}. \quad \text{(A3)}$$

With this relation, the Kramers' equation becomes

$$k(T) = a\omega_C \frac{k_B T}{h} Exp\left[-\frac{\Delta H_{Ch}^{\ddagger}}{RT} - \frac{b}{T} + \frac{\Delta S_{Ch}^{\ddagger}}{R}\right], \quad \text{(A4)}$$

where $\Delta H_{Ch}^{\ddagger}$ is the activation enthalpy and $\Delta S_{Ch}^{\ddagger}$ is the activation entropy. Here, $\Delta H_{Ch}^{\ddagger}$ and b were lumped together as $\Delta H_{Ch}'^{\ddagger}$ ($=\Delta H_{Ch}^{\ddagger} + bR$) because $\zeta(T)$ and its temperature dependence cannot be obtained unequivocally. Also, a and ω_C were collected as ω_C' ($=a\omega_C$). Then,

$$k(T) = \omega_C' \frac{k_B T}{h} Exp\left[-\frac{\Delta H_{Ch'}^{\ddagger}}{RT} + \frac{\Delta S^{\ddagger}}{R}\right]. \quad \text{(A5)}$$

The temperature dependence of $k(T)$, or Q_{10} of proton permeation, is expressed as:

$$Q_{10}(T) = Exp[10 \times \partial_T \log k(T)] = Exp\left[10 \times \left(\frac{\Delta H_{Ch'}^{\ddagger}}{RT^2} + \frac{1}{T}\right)\right]. \quad \text{(A6)}$$

The access resistance

Access resistance was formalized theoretically based on geometrical and electrostatic considerations, and a simplified expression was proposed by Hall (1975) as

$$R_{AR} = \frac{\rho}{4r}, \quad \text{(A7)}$$

where ρ is the resistivity of the solution and r is the capture radius. The resistance of a hemispherical region outside a pore entrance was integrated to give the access resistance, and most of the resistance arises within close vicinity of the pore. The time for development of the access resistance can be estimated by r^2/D (Crank, 1975). For $r < 1$ nm and D (diffusion coefficient) $< 10^{-4}$ cm^2/s, the time constant is 10^{-10} s.

The access resistance is further modified by the presence of buffer. Protonated buffer distributes within the access region and supplies protons to the pore, which replenishes the limited delivery (proton supply by buffer; Fig. 2) (Decker and Levitt, 1988). This may attenuate amplitudes of the access resistance. Here, we estimate the effectiveness of the proton supply from the buffer to the pore quantitatively. The time constant for buffering is

$$\frac{1}{k_1[H^+] + k_{-1}},$$

and it is calculated as 10^{-4} to 10^{-5} s for a k_1 of 10^9–10^{10} M^{-1}/s and k_{-1} of $k_1 \times 10^{-pK}$. This value is much larger than the time constant for development of the access resistance ($\sim 10^{-10}$ s). This means that the release rate of protons from the protonated buffer is much slower than the development of access resistance. In this case, the proton supply from the protonated buffer cannot keep up with the demand. The access resistance for the voltage-gated proton channel has not been estimated quantitatively, so these theoretical predictions remain to be evaluated experimentally.

The total resistance (R_{total}) across the membrane is composed of the channel resistance (R_{Ch}) and the access resistance on both sides of the membrane (external and internal R_{AR}).

$$R_{total} = R_{Ch} + R_{AR}^{i} + R_{AR}^{o}. \quad \text{(A8)}$$

The relative contributions of R_{AR} to R_{total} were estimated by the following methods. Changes in the external R_{AR} lead to changes in R_{total}, even if R_{Ch} and internal R_{AR} are constant. The external R_{AR} can be changed by altering ρ (Eq. A7) (Hall, 1975), which is attained by perfusing extracellular solutions with higher resistivity, such as by adding concentrated nonelectrolytes (Ando et al., 2005). From the changes in the current amplitude upon exposure (the resistivity pulse method), the relative contribution of R_{AR} to R_{Ch} can be estimated by this equation:

$$\frac{I^{jump}}{I^{pre-jump}} = \frac{R_{Ch} + R_{AR}^{o} + R_{AR}^{i}}{R_{Ch} + R_{AR}^{o\prime} + R_{AR}^{i}}, \quad \text{(A9)}$$

in which $R_{AR}^{o\prime}$ represents the resistance after perfusion with a different conductivity solution. Incorporating Hall's relation for the ratio of the access resistances at different solutions, the conductance ratio can be obtained:

$$\frac{I^{jump}}{I^{pre-jump}} = \frac{1 + \dfrac{R_{Ch} + R_{AR}^{i}}{R_{AR}^{o}}}{\dfrac{R_{Ch} + R_{AR}^{i}}{R_{AR}^{o}} + \dfrac{\rho'}{\rho}}. \quad \text{(A10)}$$

We assume that the external and internal R_{AR} are identical in symmetric solutions. Based on Hall's equation, R_{AR} is determined by the conductivity and the capture radius. Therefore, the symmetric assumption is acceptable as far as the structural information of the channel is not available. Eq. A10 becomes

$$\frac{I^{jump}}{I^{pre-jump}} = \frac{2 + R_{Ch}/R_{AR}}{1 + R_{Ch}/R_{AR} + \rho'/\rho}. \quad \text{(A11)}$$

Published August 31, 2009

In this equation, the resistivities of the buffer solution were measured by a conductivity meter at different temperatures. The resistance ratio is an only unknown parameter that can be obtained through fitting the experimental data.

The Q_{10} value for resistances in series

The total conductance of the channel and access resistances in series are expressed as

$$G_{total} = \frac{G_{Ch} \times G_{AR}}{G_{AR} + 2G_{Ch}}, \tag{A12}$$

where G_{Ch} is the channel conductance and G_{AR} is the access conductance. The Q_{10} value for this conductance is

$$Q_{10}(T) = Exp\left[10 \times \partial_T \log(G_{total})\right] = Exp\left[10 \times \frac{2G_{Ch}G_{AR}' + G_{AR}^2 G_{Ch}'}{G_{AR}^2 G_{Ch} + 2G_{AR}G_{Ch}^2}\right]. \tag{A13}$$

G_{Ch} was replaced by $k(T)$ and G_{AR} was replaced by Eq. 12, in which ρ is expressed by $1/(A\,\mathrm{Exp}[-B/T])$. Then, $Q_{10}(T)$ is expressed as

$$Q_{10} = Exp\left[\frac{10}{T^2}\left(B + \frac{A\left(\frac{\Delta H_{Ch}^{\ddagger}}{R} + T - B\right)Exp\left[\frac{\Delta H_{Ch}^{\ddagger}}{RT}\right]}{AExp\left[\frac{\Delta H_{Ch}^{\ddagger}}{RT}\right] + 2\omega_C \frac{k_B T}{h} Exp\left[\frac{\Delta S_{Ch}^{\ddagger}}{R} + \frac{B}{T}\right]}\right)\right], \tag{A14}$$

where $\Delta H_{Ch}^{\ddagger}$ is the activation enthalpy, $\Delta S_{CH}^{\ddagger}$ is the activation entropy, and ω_C is the frequency factor for the channel. A and B can be obtained from the resistivity measurements at different temperatures. The fitting of the three unknown parameters ($\Delta H^{\ddagger}_{Ch}$, $\Delta S^{\ddagger}_{Ch}$, and ω_C) to the measured Q_{10} values was performed.

We would like to thank O.S. Andersen, M. Iwamoto, T. Konno, H. Shimizu, S. Irie, and C. Edwards for discussion. We also thank J. Kawawaki and H. Nakagawa for technical assistance and T. Goto for secretarial assistance.

This work is supported by a Grant-in-Aid for Scientific Research from the Ministry of Education, Culture, Sports, Science and Technology (Japan).

Lawrence G. Palmer served as editor.

Submitted: Submitted: 3 February 2009
Accepted: Accepted: 23 July 2009

REFERENCES

Agmon, N. 1995. The Grotthuss mechanism. *Chem. Phys. Lett.* 244:456–462.

Agmon, N. 1996. Hydrogen bonds, water rotation and proton mobility. *J. Chim. Phys.* 93:1714–1736.

Agmon, N. 1999. Proton solvation and proton mobility. *Isr. J. Chem.* 39:493–502.

Aguilella-Arzo, M., V.M. Aguilella, and R.S. Eisenberg. 2005. Computing numerically the access resistance of a pore. *Eur. Biophys. J.* 34:314–322.

Akeson, M., and D.W. Deamer. 1991. Proton conductance by the gramicidin water wire. Model for proton conductance in the F1F0 ATPases? *Biophys. J.* 60:101–109.

Andersen, O.S. 1983. Ion movement through gramicidin A channels. Studies on the diffusion-controlled association step. *Biophys. J.* 41:147–165.

Andersen, O.S. 1984. Gramicidin channels. *Annu. Rev. Physiol.* 46:531–548.

Ando, H., M. Kuno, H. Shimizu, I. Muramatsu, and S. Oiki. 2005. Coupled K+–water flux through the HERG potassium channel measured by an osmotic pulse method. *J. Gen. Physiol.* 126:529–538.

Bamberg, E., and P. Läuger. 1974. Temperature-dependent properties of gramicidin A channels. *Biochim. Biophys. Acta.* 367:127–133.

Berg, H.C., and E.M. Purcell. 1977. Physics of chemoreception. *Biophys. J.* 20:193–219.

Berry, R.S., S.A. Rice, and J. Ross. 2000. Physical Chemistry. 2nd Ed. Oxford University Press, New York. 1080 pp.

Braun-Sand, S., A. Burykin, Z.T. Chu, and A. Warshel. 2005. Realistic simulations of proton transport along the gramicidin channel: demonstrating the importance of solvation effects. *J. Phys. Chem. B.* 109:583–592.

Byerly, L., and Y. Suen. 1989. Characterization of proton currents in neurones of the snail, Lymnaea stagnalis. *J. Physiol.* 413:75–89.

Cherny, V.V., R. Murphy, V. Sokolov, R.A. Levis, and T.E. DeCoursey. 2003. Properties of single voltage-gated proton channels in human eosinophils estimated by noise analysis and by direct measurement. *J. Gen. Physiol.* 121:615–628.

Chernyshev, A., and S. Cukierman. 2002. Thermodynamic view of activation energies of proton transfer in various gramicidin A channels. *Biophys. J.* 82:182–192.

Crank, J. 1975. The Mathematics of Diffusion. 2nd Ed. Clarendon Press, Oxford, UK. 424 pp.

Cukierman, S. 2000. Proton mobilities in water and in different stereoisomers of covalently linked gramicidin A channels. *Biophys. J.* 78:1825–1834.

Day, T.J.F., U.W. Schmitt, and G.A. Voth. 2000. The mechanism of hydrated proton transfer in water. *J. Am. Chem. Soc.* 122:12027–12028.

de Grotthuss, C.J.T. 1806. Sur la décomposition de l'eau et des corp qu'elle tient en dissolution à l'aide de l'électricité galvanique. *Annales de Chimie.* LVIII:54–74.

Decker, E.R., and D.G. Levitt. 1988. Use of weak acids to determine the bulk diffusion limitation of H^+ ion conductance through the gramicidin channel. *Biophys. J.* 53:25–32.

DeCoursey, T.E. 2003. Voltage-gated proton channels and other proton transfer pathways. *Physiol. Rev.* 83:475–579.

DeCoursey, T.E. 2008. Voltage-gated proton channels: what's next? *J. Physiol.* 586:5305–5324.

DeCoursey, T.E., and V.V. Cherny. 1996. Effects of buffer concentration on voltage-gated H^+ currents: does diffusion limit the conductance? *Biophys. J.* 71:182–193.

DeCoursey, T.E., and V.V. Cherny. 1998. Temperature dependence of voltage-gated H^+ currents in human neutrophils, rat alveolar epithelial cells, and mammalian phagocytes. *J. Gen. Physiol.* 112:503–522.

Eigen, M. 1964. Proton transfer, acid-base catalysis, and enzymatic hydrolysis. Part 1: elementary processes. *Angew. Chem. Int. Ed. Engl.* 3:1–72.

Eigen, M., W. Kruse, G. Maass, and L. De Maeyer. 1964. Rate constants of proteolytic reactions in aqueous solution. *Prog. React. Kinet.* 2:287–318.

Fersht, A. 1999. Structure and Mechanism in Protein Science. W.H. Freeman and Company, New York. 650 pp.

Published August 31, 2009

Gordienko, D.V., M. Tare, S. Parveen, C.J. Fenech, C. Robinson, and T.B. Bolton. 1996. Voltage-activated proton current in eosinophils from human blood. *J. Physiol.* 496:299–316.

Grygorczyk, R. 1987. Temperature dependence of Ca^{2+}-activated K^+ currents in the membrane of human erythrocytes. *Biochim. Biophys. Acta.* 902:159–168.

Gutfreund, H. 1995. Kinetics for the Life Sciences: Receptors, Transmitters and Catalysts. Cambridge University Press, Cambridge, UK. 346 pp.

Hall, J.E. 1975. Access resistance of a small circular pore. *J. Gen. Physiol.* 66:531–532.

Hänggi, P., P. Talkner, and M. Borkovec. 1990. Reaction-rate theory: fifty years after Kramers. *Rev. Mod. Phys.* 62:251–341.

Heinemann, S.H., and F.J. Sigworth. 1989. Estimation of Na^+ dwell time in the gramicidin A channel. Na^+ ions as blockers of H^+ currents. *Biochim. Biophys. Acta.* 987:8–14.

Henderson, L.M., J.B. Chappell, and O.T. Jones. 1987. The superoxide-generating NADPH oxidase of human neutrophils is electrogenic and associated with an H^+ channel. *Biochem. J.* 246:325–329.

Hille, B. 1968. Pharmacological modifications of the sodium channels of frog nerve. *J. Gen. Physiol.* 51:199–219.

Hille, B. 2001. Ion Channels of Excitable Membranes. 3rd Edition. Sinauer Associates Inc., Sunderland, MA. 814 pp.

Hladky, S.B. 1984. Ion currents through pores. The roles of diffusion and external access steps in determining the currents through narrow pores. *Biophys. J.* 46:293–297.

Hoffmann, H.M., and V.E. Dionne. 1983. Temperature dependence of ion permeation at the endplate channel. *J. Gen. Physiol.* 81:687–703.

Keener, J., and J. Sneyd. 1998. Mathematical Physiology. Springer-Verlag, New York. 792 pp.

Koeppe, R.E.I.I., II, and O.S. Anderson. 1996. Engineering the gramicidin channel. *Annu. Rev. Biophys. Biomol. Struct.* 25:231–258.

Kramers, H.A. 1940. Brownian motion in a field of force and the diffusion model of chemical reactions. *Physica.* 7:284–304.

Kuno, M., J. Kawawaki, and F. Nakamura. 1997. A highly temperature-sensitive proton current in mouse bone marrow–derived mast cells. *J. Gen. Physiol.* 109:731–740.

Läuger, P. 1976. Diffusion-limited ion flow through pores. *Biochim. Biophys. Acta.* 455:493–509.

Limbach, H.H., J. Miguel Lopez, and A. Kohen. 2006. Arrhenius curves of hydrogen transfers: tunnel effects, isotope effects and effects of pre-equilibria. *Philos. Trans. R. Soc. Lond. B Biol. Sci.* 361:1399–1415.

Mahaut-Smith, M.P. 1989. The effect of zinc on calcium and hydrogen ion currents in intact snail neurones. *J. Exp. Biol.* 145:455–464.

Milburn, T., D.A. Saint, and S.H. Chung. 1995. The temperature dependence of conductance of the sodium channel: implications for mechanisms of ion permeation. *Receptors Channels.* 3:201–211.

Miller, C., N. Stahl, and M. Barrol., 1988. A thermodynamic analysis of monovalent cation permeation through a K(+)-selective ion channel. *Neuron.* 1:159–164.

Morgan, D., V.V. Cherny, R. Murphy, W. Xu, L.L. Thomas, and T.E. DeCoursey. 2003. Temperature dependence of NADPH oxidase in human eosinophils. *J. Physiol.* 550:447–458.

Morihata, H., J. Kawawaki, H. Sakai, M. Sawada, T. Tsutada, and M. Kuno. 2000a. Temporal fluctuations of voltage-gated proton currents in rat spinal microglia via pH-dependent and -independent mechanisms. *Neurosci. Res.* 38:265–271.

Morihata, H., F. Nakamura, T. Tsutada, and M. Kuno. 2000b. Potentiation of a voltage-gated proton current in acidosis-induced swelling of rat microglia. *J. Neurosci.* 20:7220–7227.

Oiki, S., R.E. Koeppe II, and O.S. Andersen. 1995. Voltage-dependent gating of an asymmetric gramicidin channel. *Proc. Natl. Acad. Sci. USA.* 92:2121–2125.

Peskoff, A., and D.M. Bers. 1988. Electrodiffusion of ions approaching the mouth of a conducting membrane channel. *Biophys. J.* 53:863–875.

Ramsey, I.S., M.M. Moran, J.A. Chong, and D.E. Clapham. 2006. A voltage-gated proton-selective channel lacking the pore domain. *Nature.* 440:1213–1216.

Robinson, R.A., and R.H. Stokes. 2002. Electrolyte Solutions. 2nd Revised Ed. Dover Publications, Mineola, NY. 590 pp.

Sasaki, M., M. Takagi, and Y. Okamura. 2006. A voltage sensor-domain protein is a voltage-gated proton channel. *Science.* 312:589–592.

Sawada, M., F. Imai, H. Suzuki, M. Hayakawa, T. Kanno, and T. Nagatsu. 1998. Brain-specific gene expression by immortalized microglial cell-mediated gene transfer in the mammalian brain. *FEBS Lett.* 433:37–40.

Schumaker, M.F. 2003. Numerical framework models of single proton conduction through gramicidin. *Front. Biosci.* 8:s982–s991.

Schumaker, M.F., R. Pomès, and B. Roux. 2000. A combined molecular dynamics and diffusion model of single proton conduction through gramicidin. *Biophys. J.* 79:2840–2857.

Sitsapesan, R., R.A. Montgomery, K.T. MacLeod, and A.J. Williams. 1991. Sheep cardiac sarcoplasmic reticulum calcium-release channels: modification of conductance and gating by temperature. *J. Physiol.* 434:469–488.

Starace, D.M., and F. Bezanilla. 2004. A proton pore in a potassium channel voltage sensor reveals a focused electric field. *Nature.* 427:548–553.

Stojilkovic, K.S., A.M. Berezhkovskii, V.Y. Zitserman, and S.M. Bezrukov. 2003. Conductivity and microviscosity of electrolyte solutions containing polyethylene glycols. *J. Chem. Phys.* 119:6973–6978.

Swanson, J.M.J., C.M. Maupin, H. Chen, M.K. Petersen, J. Xu, Y. Wu, and G.A. Voth. 2007. Proton solvation and transport in aqueous and biomolecular systems: insights from computer simulations. *J. Phys. Chem. B.* 111:4300–4314.

Swietach, P., M. Zaniboni, A.K. Stewart, A. Rossini, K.W. Spitzer, and R.D. Vaughan-Jones. 2003. Modelling intracellular H^+ ion diffusion. *Prog. Biophys. Mol. Biol.* 83:69–100.

Thomas, R.C., and R.W. Meech. 1982. Hydrogen ion currents and intracellular pH in depolarized voltage-clamped snail neurones. *Nature.* 299:826–828.

Urry, D.W., S. Alonso-Romanowski, C.M. Venkatachalam, R.J. Bradley, and R.D. Harris. 1984. Temperature dependence of single channel currents and the peptide libration mechanism for ion transport through the gramicidin A transmembrane channel. *J. Membr. Biol.* 81:205–217.

Zifarelli, G., P. Soliani, and M. Pusch. 2008. Buffered diffusion around a spherical proton pumping cell: a theoretical analysis. *Biophys. J.* 94:53–62.

J Mol Neurosci
DOI 10.1007/s12031-009-9187-6

Interleukin-6 Induces Prostaglandin E_2 Synthesis in Mouse Astrocytes

Toshiyuki Chikuma · Tetsuya Yoshimoto · Masahiro Ohba · Makoto Sawada · Takeshi Kato · Tomoaki Sakamoto · Yukio Hiyama · Hiroshi Hojo

Received: 9 November 2008 / Accepted: 16 February 2009

Abstract The physiological function of interleukin-6 within the central nervous system (CNS) is complex; interleukin-6 exerts neurotrophic and neuroprotective effects and yet can also function as a mediator of inflammation, demyelination, and astrogliosis depending on the cellular context. However, the roles of interleukin-6 in astrocytes are poorly understood. In the present study, we investigated the effect of the pro-inflammatory cytokine interleukin-6 on the production of the inflammatory mediator prostaglandin E_2 in mouse astrocytes. Interleukin-6 stimulated prostaglandin E_2 production in a time-dependent fashion via a rapid and transient induction of cyclooxygenase-2 messneger RNA, followed by cyclooxygenase-2 protein synthesis. Interleukin-6 may act on the nervous system by interacting with its specific soluble interleukin-6 receptor and the signal transducer 130-kDa glycoprotein. Simultaneous treatment of astrocytes with interleukin-6 and soluble interleukin-6 receptor caused marked induction of prostaglandin E_2 synthesis, and this effect was suppressed by adding a neutralizing antibody against soluble interleukin-6 receptor. Furthermore, the mouse 130-kDa glycoprotein antibody suppressed prostaglandin E_2 formation induced by interleukin-6, as well as interleukin-6/soluble interleukin-6 receptor complexes, in a dose-dependent manner. These results indicate that interleukin-6/soluble interleukin-6 receptor complexes and the signal transducer 130-kDa glycoprotein play an important role in the regulation of cyclooxygenase-2 expression and subsequent prostaglandin E_2 formation in mouse astrocytes and that interleukin-6 is an important regulator of immune and inflammatory processes in the CNS.

Keywords Interleukin-6 · Prostaglandin E_2 · Cyclooxygenase-2 · Soluble interleukin-6 receptor · 130-kDa glycoprotein · Astrocytes

Abbreviations

AD	Alzheimer's disease
ALS	Amyotrophic lateral sclerosis
bFGF	Basic fibroblast growth factor
COX	Cyclooxygenase
$cPLA_2$	Cytosolic phospholipase A_2
MEM	Minimum essential medium
EIA	Enzyme immunoassay
FBS	Fetal bovine serum
gp130	130-kDa glycoprotein
IL-1 β	Interleukin-1β
IL-6	Interleukin-6
IL-6R	Interleukin-6 receptor

T. Chikuma · T. Yoshimoto · M. Ohba · H. Hojo
Department of Hygienic Chemistry,
Showa Pharmaceutical University,
Machida-shi,
Tokyo 194-8543, Japan

M. Sawada
Department of Brain Life Science, Research Institute of Environmental Medicine, Nagoya University,
Nagoya 464-8601, Japan

T. Kato
Laboratory of Molecular Recognition, Graduate School of Integrated Science, Yokohama City University,
Yokohama 236-0027, Japan

T. Sakamoto · Y. Hiyama
Division of Drugs, National Institute of Health Sciences,
Tokyo 158-8501, Japan

T. Chikuma (✉)
Department of Pharmaceutical Analytical Chemistry,
Showa Pharmaceutical University,
3-3165 Higashi-tamagawagakuen, Machida-shi,
Tokyo 194-8543, Japan
e-mail: chikuma@ac.shoyaku.ac.jp

Published online: 10 March 2009

JAK	Janus kinase
LPS	Lipopolysaccharide
PBS	Ca^{2+}- and Mg^{2+}-free phosphate-buffered saline
PDGF	Platelet-derived growth factor
PGE_2	Prostaglandin E_2
PGs	Prostaglandins
sIL-6R	Soluble interleukin-6 receptor
STAT	Signal transducers and activators of transcription
TGF-β	Transforming growth factor-β
TNF-α	Tumor necrosis factor-α
TPBS	PBS containing 0.05% Tween 20

Introduction

Prostaglandins (PGs) are major lipid mediators produced by cyclooxygenase (COX) activity. They play important modulatory roles in various cells throughout the body. Prostaglandin E_2 (PGE_2) is the most abundant prostaglandin in the brain (Bishai and Coceani 1992) and is considered to play an essential role in several pathological states. In the central nervous system (CNS), PGE_2 is responsible for fever induction (Ushikubi et al. 1998) and participates in eliciting pain hypersensitivity (Samad et al. 2001). In addition, elevated PGE_2 levels have been detected in the cerebrospinal fluid of patients with Alzheimer's disease (AD; Montine et al. 1999), stroke (Jacobs et al. 1987), ischemia (Nogawa et al. 1997), and amyotrophic lateral sclerosis (ALS; Almer et al. 2001). When cells and tissue are exposed to various pro-inflammatory stimuli, arachidonic acid is liberated from membrane phospholipids and converted to PGs by the action of COX enzymes.

COX is the key enzyme in the metabolic pathway leading to PG and thromboxane A_2 formation from arachidonic acid (Dubois et al. 1998). Two isoforms have been identified, COX-1 and COX-2 (Smith et al. 1996). COX-1 is constitutively expressed in nearly all normal mammalian tissues and mediates the synthesis of PGs required for physiological tissue homeostasis. By contrast, COX-2 is constitutively expressed in the brain in specific neuronal populations where it seems to be regulated by synaptic activity (Hayaishi 1991; Yamagata et al. 1993; Marcheselli and Bazan 1996). However, in inflammatory pathological conditions, the immune-competent cells of the CNS, astrocytes and microglia, are likely to be the major sources of PGs following induction of COX-2 (Minghetti and Levi 1995; O'Banion et al. 1996; Bauer et al. 1997; Vane et al. 1998; Minghetti et al. 1999; Molina-Holgado et al. 2000).

Interleukin-6(IL-6) was initially described as a central mediator of the immune system, hemopoiesis, and acute phase reaction. IL-6 is a member of the neurocytokine family, which also includes ciliary neurotrophic factor, leukemia inhibitory factor, oncostatin M, and cardiotrophin-1. These molecules have overlapping biological activities: they possess similar secondary structures and exert their activities through related multisubunit receptors (Rose-John and Heinrich 1994; Heinrich et al. 1998). The IL-6 receptor (IL-6R), gp80, can exist either as a membrane-bound protein or a soluble protein (sIL-6R; Kishimoto et al. 1994). Binding of IL-6 to either the membrane-bound or soluble form of IL-6R promotes homodimerization of a 130-kDa glycoprotein (gp130) molecule. Both neurons and glia can produce IL-6 (Gadient and Otten 1994; Sawada et al. 1995; Marz et al. 1998; Their et al. 1999).

Astrocytes are the major cell type in the CNS. These cells not only supply nutrients to neurons but also mediate inflammatory responses in the CNS. Following CNS injury or an immune/inflammatory challenge, astrocytes undergo a phenotypic alteration—a response known as activation. The activated astrocytes then release cytokines and other pro-inflammatory mediators, including PGs. These released substances communicate with such neighboring cells as neurons and microvascular cells. Astrocytes are a major source of PGs in the CNS: in culture, these cells synthesize up to 20 times more PGs than do neurons (Seregi et al. 1984). Their ability to produce PGE_2 upon stimulation with interleukin-1β (IL-1β), ATP, platelet-activating factor, transforming growth factor-β (TGF-β), oncostatin M, tumor necrosis factor-α (TNF-α), or lipopolysaccharide (LPS) has been documented (Fontana et al. 1982; O'Banion et al. 1996; Ishimoto et al. 1997; Luo et al. 1998; Mollace et al. 1998; Pistritto et al. 1998, 1999; Molina-Holgado et al. 2000; Teather et al. 2002; Repovic et al. 2003; Xu et al. 2003). However, PGE_2 formation upon stimulation of astrocytes with IL-6 has not been investigated. In the present study, we used purified mouse astrocytes to investigate the effects of IL-6 on PGE_2 synthesis and the expression of COX-2, which catalyzes PG formation. In addition, possible roles of sIL-6R and gp130 in PGE_2 formation were also explored.

Materials and Methods

Materials

PGE_2, recombinant mouse IL-6, D-glucose, and bovine pancreas insulin were purchased from Sigma Chemical Co. (St. Louis, MO, USA). DNase I and RNase inhibitor were obtained from Takara-bio Co. (Tokyo, Japan). Oligo(dt) primer and ribonuclease H were purchased from Invitrogen (Carlsbad, CA, USA). Biotin-conjugated goat anti-rabbit IgG and streptavidin–horseradish peroxidase (HRP) were obtained from Dako Cytomation (Kyoto, Japan). Anti-human sIL-6R goat antibody and anti-mouse gp130 goat antibody were purchased from R&D Systems (Minneapolis,

MN, USA). Recombinant human sIL-6R and anti-mouse COX-2 rabbit antibody were purchased from PreproTec EC Ltd. (London, UK) and Cayman Chemical Co. (Ann Arbor, MI, USA), respectively. All other reagents were purchased from commercial sources and generally were the highest purity available.

Cell Culture

Astrocytes were prepared from mixed primary glial cell cultures obtained from newborn C57BL/B6 mouse brain as previously described (Sawada et al. 1993). The purity of the astrocytes thus obtained was greater than 95%, as estimated by indirect immunofluorescence using anti-glial fibrillary acidic protein antibody. These astrocyte-enriched cultures did not contain neurofilament-positive neurons and the contamination of microglia was negligible. The cells were cultured in Eagle's minimum essential medium (Eagle's MEM; Sigma) containing 10% heat-inactivated fetal bovine serum (FBS; JRH Biosciences, Lenexa, KS, USA), 2 mg/ml glucose, 5 μg/ml bovine insulin, 100 IU/ml penicillin, and 100 μg/ml streptomycin (Gibco BRL, Rockville, MD, USA) at 37°C in an atmosphere of 5% CO_2 and 95% air and then subcultured every 3 days before the experiments were performed. For total RNA extraction, cells were plated in 10-cm diameter dishes (Falcon: 5×10^5 cells/dish in 10 ml of culture medium); for the PGE_2 enzyme immunoassay (EIA), cells were plated in 24-well plates (Iwaki: 4×10^4 cells/well in 400 μl of culture medium) and then cultured for 2 days until they were nearly confluent. The medium was then replaced with fresh medium, and cells were activated with or without various concentrations of IL-6 or other reagents followed by further culturing for the indicated periods.

Measurement of PGE_2

PGE_2 was assayed using a specific EIA system (Amersham, UK). Briefly, supernatants of cultured astrocytes or standard PGE_2 were incubated for 1 h with specific anti-PGE_2 reagent and peroxidase-labeled PGE_2 in pre-packed 96-well plates containing a goat anti-mouse solid phase. Unlabeled PGE_2 (standard or unknown) and PGE_2–peroxidase complex competed for a limited number of binding sites on PGE_2-specific antibodies, and the amount of peroxidase-labeled ligand was inversely proportional to the concentration of added standard or unknown. After washing four times with washing buffer, tetramethylbenzidine/hydrogen peroxide single pot substrate was added and incubated for 30 min. Addition of acid solution stopped the reaction, and the resultant color was read at 450 nm in a microtiter plate photometer. The concentration of unlabeled PGE_2 in a sample was determined by interpolation from a standard curve, and the data are expressed as pg PGE_2 in each well.

Western Blot Analysis

Cells were exposed to 10 ng/ml IL-6 for the indicated periods of time. Cells were washed three times with ice-cold Ca^{2+}- and Mg^{2+}-free phosphate-buffered saline (PBS) and lysed in 100 mM phosphate buffer (pH 7.4) containing 1 mM EDTA and 0.05% Triton X-100 (*v*/*v*). The cell lysates were centrifuged at 10,000×*g* for 10 min at 4°C and the resultant supernatants were used for analysis. Protein concentration was determined by the Bradford method (Bradford 1976) using bovine serum albumin as a standard protein. For Western blotting, 10 μg of cell protein from each sample for COX-2 detection was subjected to sodium dodecyl sulfate–polyacrylamide gel electrophoresis on an 8% separating gel under reducing conditions. Proteins were then transferred onto poly(vinylidene difluoride) membranes (Millipore, Bedford, MA, USA) by semi-dry blotting. The electroblotted membranes were blocked for 1 h in 2% Block Ace solution (Dainippon Pharmaceutical, Osaka, Japan) and then incubated with anti-mouse COX-2 rabbit antibody (1:32,000) for 1.5 h at room temperature. Subsequently, the membranes were washed three times in PBS containing 0.05% Tween 20 (TPBS) and incubated for 45 min with biotin-conjugated goat anti-rabbit IgG (1:50,000). After washing membranes three times with TPBS, they were incubated with streptavidin-HRP (1:50,000) for 45 min at room temperature and the resulting protein bands were visualized using ECL Plus Western blotting detection reagents (GE Healthcare Bio-Sciences, Piscataway, NJ, USA) according to the manufacturer's instructions. Immunoblots were digitized using Image-Master ID Elite (GE Healthcare Bio-Sciences) and expressed as fold induction compared with control cultures.

RNA Extraction and Reverse Transcription PCR Analysis

Total RNA was extracted from astrocytes using ISOGEN (Nippongene Co., Tokyo, Japan) according to the manufacturer's instructions. The purity of the RNA preparations was checked by measuring the absorbance ratio at 260/280 nm. Each RNA sample was subjected to first-strand complementary DNA (cDNA) synthesis using SuperScript II reverse transcriptase (Invitrogen) following the protocol suggested by the manufacturer. Reactions were performed at 42°C for 50 min. cDNA samples (0.5 μl) were amplified for 30 (β-actin) or 35 cycles (COX-2) in an Astec PC-800 thermal cycler using Taq DNA polymerase and polymerase chain reaction (PCR) reagents (Takara-bio Co.), with primers specific for β-actin and COX-2, in a total volume of 25 μl. The PCR amplimer pairs for the analysis of COX-2 cDNA were 5′-CATGGGTGTGAAGGGAAATAAG-3′ (sense) and 5′-TGAGATAGTGACCGTGGGGG-3′ (antisense), which were complementary to the conserved

regions of the cDNA for mouse COX-2 (O'Banion et al. 1992). The β-actin cDNA amplimers were 5′-GTGGGCCGGTCTAGGCACCA-3′ (sense) and 5′-GGTTGGCCTTAGGGTTCAGG-3′ (antisense; Kaartinen et al. 1995). β-actin messenger RNA (mRNA) was assessed to control for the amount and the integrity of RNA in each sample. Each PCR cycle consisted of a denaturation step (94°C for 45 s), an annealing step (60°C for 45 s), and a primer extension step (72°C for 2 min). PCR products were separated by 10% polyacrylamide gel electrophoresis and visualized by ethidium bromide staining. The densities of the bands corresponding to COX-2 and β-actin were analyzed by densitometry (NIH Image J software).

Statistical Analysis

One-way analysis of variance was carried out to determine the levels of significance in experiments. Multiple group comparisons were performed using the Student–Newman–Keuls test. Data are given as means ± SD values.

Results

IL-6 Stimulates PGE_2 Release in Cultured Mouse Astrocytes

Release of PGE_2 into the supernatants of cultured astrocytes was assayed by EIA. The dose-dependent effects of IL-6 were examined by 20-h culturing at concentrations of 0.01 to 10 ng/ml. As shown in Fig. 1a, IL-6 produced a dose-dependent increase in PGE_2 release from astrocytes; the plateau was reached at 1 ng/ml. The increase in PGE_2 release at plateau, which was about 2.5-fold over the control level, was observed at concentrations of 1 and 10 ng/ml. Based on this observation, IL-6 was used at a concentration of 10 ng/ml in further experiments unless stated otherwise. The time-dependent changes in PGE_2 release at a concentration of 10 ng/ml of IL-6 are shown in Fig. 1b. PGE_2 release increased significantly from as early as 8 h in culture and thereafter reached a maximum at 20 h in culture. These results indicate that IL-6 induces PGE_2 release in astrocytes.

IL-6 Induces COX-2 mRNA Expression in Cultured Mouse Astrocytes

To determine the mechanism by which IL-6 increases PGE_2 release into the supernatants of cultured astrocytes, we isolated RNA from astrocytes and subjected it to reverse transcriptase PCR (RT-PCR) analysis using primers for COX-2. Expression of the *β-actin* gene was used as a control for normalization. The RT-PCR analysis of RNA

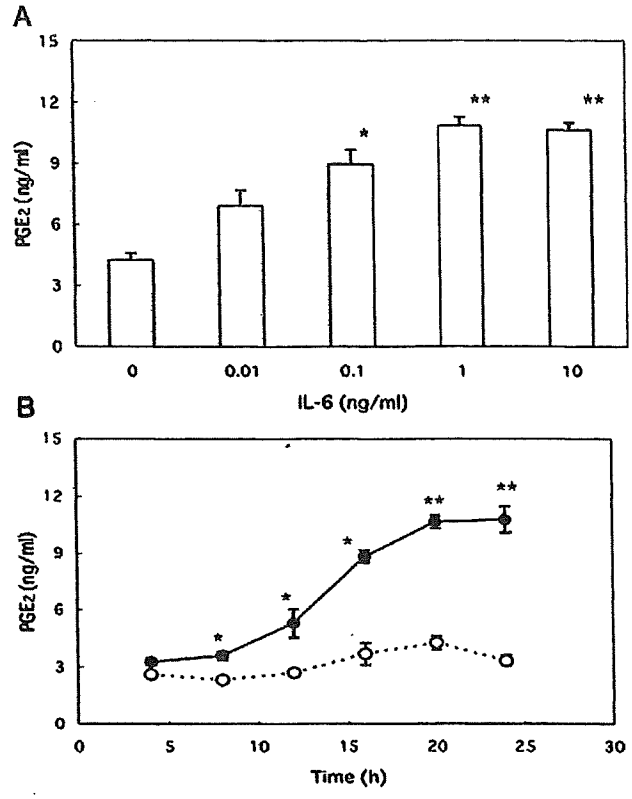

Figure 1 IL-6 induces PGE_2 release in astrocytes. Cells were treated with vehicle as a control or the indicated concentrations of IL-6 for 20 h (a). Cells were treated with vehicle as a control (*empty circle*) and 10 ng/ml IL-6 for various times as indicated (*filed circle*) (b). After incubation, the culture media were collected and the levels of PGE_2 were measured by EIA. Data are mean ± SD (*bars*) values from five independent experiments. Significant increases in PGE_2 release compared with the control are indicated by *asterisks*: $*p<0.05$, $**p<0.01$

isolated from IL-6-treated astrocytes confirmed that COX-2 mRNA was induced in mouse astrocytes by 10 ng/ml IL-6 (Fig. 2). As shown in Fig. 2, treatment with IL-6 resulted in a time-dependent expression of COX-2 mRNA. COX-2 mRNA levels increased significantly from as early as 1 h in culture and thereafter seemed to be produced at a similar level, namely 2.4-fold above the control level, until 5 h in culture; COX-2 mRNA levels returned to the control level after 6 h in culture. These data indicate that COX-2 mRNA levels are increased in IL-6-stimulated astrocytes.

IL-6 Induces COX-2 Protein Synthesis in Cultured Mouse Astrocytes

A recent study demonstrated that IL-6 mediates COX-2 induction in prostatic intraepithelial neoplasia cells (Liu et al. 2002). Therefore, we examined the effect of IL-6 on COX-2 expression by astrocytes. As shown in Fig. 3,

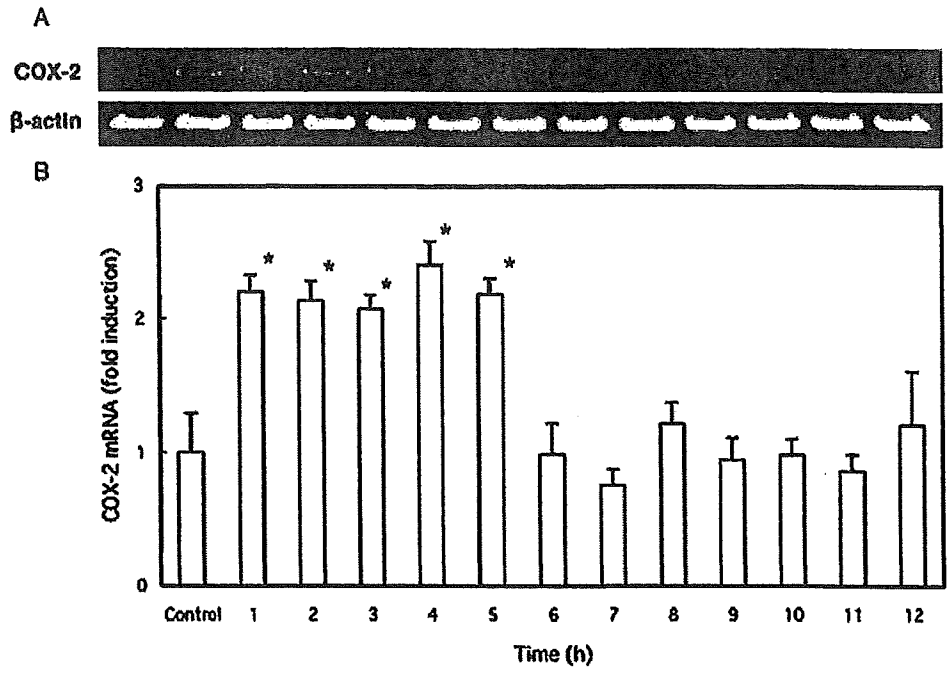

Figure 2 Time course of COX-2 mRNA induction by IL-6 in astrocytes. Cells were treated with 10 ng/ml IL-6 for the indicated times. Total RNA was isolated and the levels of mRNAs for COX-2 and β-actin were determined by RT-PCR (a). Band intensities were analyzed using Image J 1.32 software, and for each sample, COX-2 mRNA levels were normalized to the mRNA levels of the housekeeping *β-actin* gene. Data are mean ± SD (*bars*) values from five independent experiments. Values are expressed as fold induction to control cultures defined as 1.0. Significant increases in COX-2 mRNA induction compared with the control are indicated by *asterisks*: $*p<0.05$ (b)

astrocytes expressed basal levels of COX-2, and this expression was increased in the presence of 10 ng/ml IL-6. The IL-6 induction of COX-2 expression was time-dependent, with a peak increase noted 2 h after IL-6 treatment, and COX-2 expression remained elevated up to 6 h after treatment. COX-2 migrates in this electrophoretic system as a doublet (owing to glycosylation) approximately 70–72 kDa in size (Morham et al. 1995).

Effect of IL-6 in the Absence and Presence of sIL-6R on PGE_2 Release in Cultured Mouse Astrocytes

The receptor mediating the biological activities of IL-6 is composed of two subunits: IL-6R and gp130. Additionally, sIL-6R, with a molecular weight of approximately 50 kDa, was identified as a central element in the mediation of IL-6 signaling (Peters et al. 1998). To determine whether IL-6 could complex with sIL-6R and affect PGE_2 release, astrocytes were incubated with increasing concentrations of sIL-6R and sIL-6R antibodies. Figure 4a shows the effects of IL-6 on PGE_2 production when added in combination with sIL-6R to the culture. When astrocytes were treated with 10 ng/ml IL-6 in the presence of various concentrations of sIL-6R for 24 h, the release of PGE_2 was dependent on the concentration of sIL-6R (0.01–100 ng/ml): the maximum increase in PGE_2 release, which was about 5.3-fold over the control level (17.83±5.52 ng/ml), was observed at a concentration of 100 ng/ml sIL-6R. Figure 4b shows the effects of a neutralizing antibody against human sIL-6R on PGE_2 formation induced by 10 ng/ml IL-6 in a 24-h culture. The human sIL-6R antibody suppressed the PGE_2 formation induced by IL-6 in a dose-dependent manner (0.01–10 μg/ml). The effective suppression of PGE_2 release induced by sIL-6R antibody was observed at concentrations of 1 and 10 μg/ml. These results indicate that IL-6/sIL-6R complexes stimulate PGE_2 release in cultured astrocytes.

Effect of a Neutralizing Antibody against gp130 on PGE_2 Release in Cultured Mouse Astrocytes

The first step in the IL-6 transducing mechanisms is the binding of the cytokine to its specific receptor subunit followed by the association of a second subunit, the signal transducer gp130 (Hibi et al. 1990). To determine whether IL-6-induced PGE_2 release is coupled with gp130, astrocytes were incubated with increasing concentrations of an anti-mouse gp130 antibody. Figure 5 shows the effect of this neutralizing antibody against mouse gp130 on PGE_2 formation induced by IL-6 and sIL-6R in a 24-h culture. As the maximum effect on PGE_2 release induced by IL-6 was observed at a concentration of 1 ng/ml (Fig. 1a), cells were treated with 1 ng/ml IL-6 in the presence of various concentrations of gp130 antibody, with or without 100 ng/ml sIL-6R. The mouse gp130 antibody suppressed the PGE_2 formation induced by IL-6 as well as IL-6/sIL-6R complexes in a dose-dependent manner (0.01–10 μg/ml): the maximum suppressions on PGE_2 release induced by IL-6 and IL-6/sIL-6R complexes, which were about 77.7% and 68.3% compared with the control levels, respectively, were

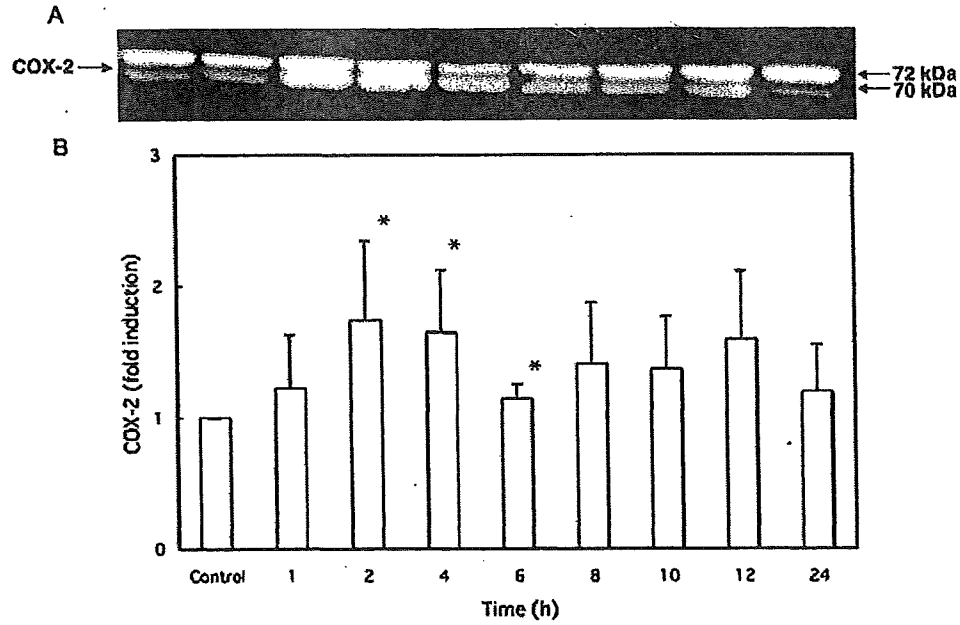

Figure 3 Time course of COX-2 protein induction by IL-6 in astrocytes. Cells were treated with 10 ng/ml IL-6 for the indicated times. Then, cell lysates were prepared and Western blot analysis was performed as described in the "Materials and Methods". A typical Western blot pattern of COX-2 is shown in a. The approximate sizes of glycosylated and unglycosylated COX-2 proteins are indicated on the *right*. A quantitative assay of Western blotting was performed using ImageMaster ID Elite. Data are mean ± SD (*bars*) values from four independent experiments. Values are expressed as fold induction to control cultures defined as 1.0. Significant increases in COX-2 protein induction compared with the control are indicated by *asterisks*: $*p<0.05$

observed in the presence of the gp130 antibody at a concentration of 10 μg/ml. As shown in Fig. 5, treatment with gp130 antibody resulted in a decrease in PGE_2 release at concentrations of 1 and 10 μg/ml in non-treated cells (control). These results may be the effect of the gp130 antibody on other stimulants.

Discussion

Astrocyte activation occurs during immune reactions (Saas et al. 2000), and these activated cells synthesize and release such inflammatory compounds as IL-1β and PGs (Dayton and Major 1996). Inflammation-related events appear to have a significant role in the progression and propagation of the neurodegenerative processes in AD (McGeer et al. 1990) and ALS (Almer et al. 2001). Interestingly, the levels of PGs and/or the enzymes involved in PG production are increased in ALS (Almer et al. 2001) and AD (Stephenson et al. 1996). A role for astrocyte-derived PGs in neuronal cell death has been demonstrated. For example, PGE_2 stimulates astrocytic glutamate release and prevents astrocytes from taking up glutamate (Bezzi et al. 1998; Pasti et al. 2001); the consequent increase in extracellular glutamate is neurotoxic (Drachman and Rothstein 2000). These results suggest that astrocytes (and the substances they release) may be a critical component in the mechanisms underlying neurodegeneration. Astrocytes are a major source of PGs in the CNS. Their ability to produce PGE_2 upon stimulation with several stimulants has been reported. For example, LPS and TGF-β caused a concentration-dependent increase in PGE_2 production in primary cultures of rat astrocytes (Luo et al. 1998; Pistritto et al. 1999). Increased production of PGE_2 after stimulation with IL-1β has also been shown in murine astrocytes (O'Banion et al. 1996). Repovic et al. (2003) demonstrated that oncostatin M synergistically upregulates PGE_2 production induced by the pro-inflammatory mediators IL-1 β, TNF-α, and LPS in astrocytes and astroglioma cells. In this report, we demonstrate that IL-6 increases PGE_2 levels at concentrations of 0.1–10 ng/ml and in time-dependent manners in cultured mouse astrocytes (Fig. 1a, b). Since PGE_2 is freely permeable and cannot be stored intracellularly, the observed rise in PGE_2 level is likely to be due to its de novo synthesis (Smith et al. 2000).

Intracellular PGE_2 synthesis requires three classes of enzymes: phospholipase A_2, COX, and PGE_2 synthase. Each of these enzymes has at least two different isoforms, which may be differently expressed in various cell types. Two COX enzymes have been identified thus far. COX-1 is constitutively expressed and largely responsible for baseline prostaglandin production (DeWitt and Smith 1988). COX-2

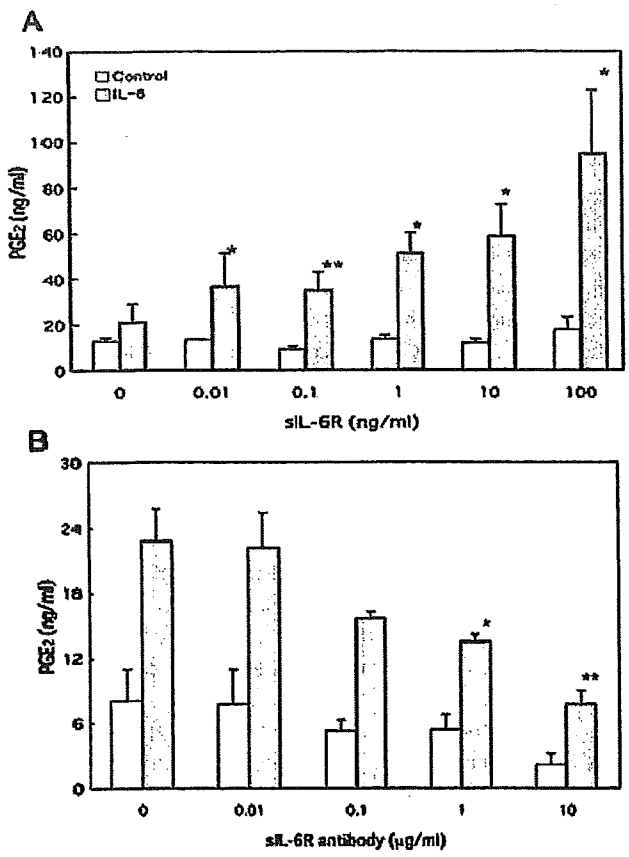

Figure 4 PGE_2 induction by IL-6 in the presence of sIL-6R in astrocytes. Cells were treated with vehicle as a control or 10 ng/ml IL-6 in the presence of various concentrations of sIL-6R (**a**) or sIL-6R antibody (**b**) for 24 h. After incubation, the culture media were collected and the levels of PGE_2 were measured by EIA. Data are mean ± SD (*bars*) values from five independent experiments. Significant increases in PGE_2 release compared with the control are indicated by *asterisks* (**a**); significant decreases in PGE_2 release compared with unstimulated cells are also indicated by *asterisks* (**b**): $*p<0.05$, $**p<0.01$

is the major inducible form of COX and is associated with delayed prostaglandin production (Xie et al. 1991; Kudo and Murakami 1999). In mouse astrocytes treated with IL-6, COX-2 mRNA and protein levels are highly upregulated in medium supplemented with 10% FBS (Figs. 2 and 3). Thus, IL-6-enhanced PGE_2 production is mediated by the stimulatory effect of IL-6 on the expression of COX-2. The present report confirms the results of other studies (Luo et al. 1998; Repovic et al. 2003; Xu et al. 2003) by showing that cultured astrocytes express the inducible COX and secrete PGE_2. On the other hand, O'Banion et al. (1996) demonstrated that IL-1β and phorbol 12-myristate 13-acetate, as well as LPS, TNF-α, and basic fibroblast growth factor (bFGF), but not IL-6, caused a significant accumulation of COX-2 mRNA in astrocytes cultured in serum-free medium. A possible explanation for this discrepancy is as follows. The production of PGs is affected by the serum content of the medium. For example, in osteoblasts and vascular smooth myocytes, serum induces a rapid increase in the expression level of COX-2, but has little effect on COX-1 expression (Pilbeam et al. 1993; Pritchard et al. 1994). FBS contains various mitogenic growth factors, such as bFGF, epidermal growth factor, insulin-like growth factor, and platelet-derived growth factor (PDGF). PDGF can upregulate the mRNA for COX in fibroblasts (Lin et al. 1989). Thus, it is conceivable that these mitogenic growth factors mediate the increase in the expression level of COX-2.

In this report, by 5-h culture, the time needed for maximal expression of COX-2, there was no PGE_2 synthesis. On the other hand, at the time point where PGE_2 is detected (8–24 h culture), there is no COX-2 expression (Figs. 1 and 2). A possible explanation for this discrepancy is as follows. In mammalian cells, prostaglandin-biosynthetic pathways utilizing endogenous arachidonic acid are subdivided into three distinct phases which show different kinetics and possible recruitment of different sets of biosynthetic enzymes. The constitutive immediate response, which occurs within several minutes after stimuli causing a rapid and transient increase in cytoplasmic Ca^{2+}, is regulated by posttranslational activation of constitutively expressed enzymes. The delayed response, which proceeds gradually for several hours after pro-inflammatory stimuli, requires de novo synthesis of particular biosynthetic enzymes. The induced immediate response, which is elicited by Ca^{2+}-mobilizing stimuli after priming by pro-inflammatory stimuli, reflects the combination of the above two responses and involves both

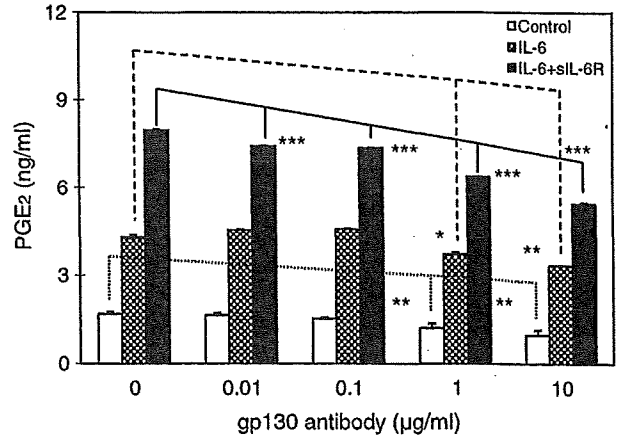

Figure 5 Participation of gp130 in the induction of PGE_2 expression in astrocytes. Cells were treated with 1 ng/ml IL-6 in the presence of various concentrations of gp130 antibody, with or without 100 ng /ml sIL-6R for 24 h. After incubation, the culture media were collected and the levels of PGE_2 were measured by EIA. Data are mean ± SD (*bars*) values from four independent experiments. Significant increases in PGE_2 release compared with the control are indicated by asterisks: $*p<0.05$, $**p<0.01$, $***p<0.001$

constitutive and inducible enzymes. For example, rat peritoneal macrophages treated with LPS predominantly produced PGE_2 during culture for 6–24 h by the delayed response. Delayed PGE_2 generation was accompanied by increasing expression of cytosolic phospholipase A_2 ($cPLA_2$) and de novo induction of COX-2. In the delayed response, $cPLA_2$ and type IIA secretory phospholipase A_2 function cooperatively with inducible COX-2, which was in turn coupled with PGE_2 synthase. COX-1 was non-functional in the delayed response, even though it was constitutively expressed in the cell (Kudo and Murakami 1999). In mouse astrocytes treated with IL-6, PGE_2 synthesis may be regulated by the delayed response.

Cells responsive to IL-6 express on their surface a low affinity receptor that does not have transducing activity. The IL-6/IL-6R complexes induces the homodimerization of a signal-transducing component, gp130, leading to cytoplasmic signaling cascades that activate components of the Janus kinase (JAK)/signal transducers and activators of transcription (STAT) pathway, particularly the activation of the transcription factor STAT-3 (Taga and Kishimoto 1997). sIL-6R can be generated by shedding of the membrane-bound receptor (Mullberg et al. 1993, 1994) or by alternative splicing of mRNA (Lust et al. 1992). Since the transmembrane and cytoplasmic regions of the IL-6R are not essential for signal transduction, sIL-6R can form a complex with IL-6 in solution and associate with gp130, thereby activating signal transduction. Previously, Oh et al. (1998) showed that human astrocytes express low levels of IL-6R and require the addition of sIL-6R for IL-6-mediated responses. Herein, we have shown that treatment of murine astrocytes with IL-6 and sIL-6R leads to marked induction of PGE_2 synthesis, and this effect was suppressed by adding a neutralizing antibody against sIL-6R (Fig. 4). These results suggest that sIL-6R plays a pivotal role in determining the level of PGE_2 synthesis by astrocytes in the CNS and furthermore influences IL-6 function in the CNS. This is supported by several reports that CNS cells that are normally slightly responsive or unresponsive to IL-6 become responsive on addition of sIL-6R. In human astrocytes, IL-6 alone has no effect on α_1-antichymotrypsin expression, whereas addition of sIL-6R leads to its expression (Kordula et al. 1998). In the presence of sIL-6R, IL-6 inhibits TNF-α-induced VCAM-1 expression in astrocytes (Oh et al. 1998). These findings suggest that sIL-6R is a functionally relevant CNS molecule. It is not clear if addition of a neutralizing antibody against sIL-6R to sIL-6R will have any effect on IL-6-induced stimulation of PGE_2 synthesis where exogenous sIL-6R is not added. However, Fig. 4a, b indicates that IL-6/sIL-6R complexes stimulate PGE_2 release in cultured mouse astrocytes.

Gp130, a protein associated with the IL-6/sIL-6R complexes, is a signal-transducing receptor shared by members of the IL-6 cytokine family comprising IL-6, interleukin-11, leukemia inhibitory factor, oncostatin M, ciliary neurotrophic factor, and cardiotrophin-1 (Taga and Kishimoto 1997). The JAK/STAT pathway, an important signal pathway downstream of gp130, has been implicated in diverse pathophysiological processes such as ischemia (Justicia et al. 2000; Choi et al. 2003a, b), inflammation associated with astroglial activation (Gautron et al. 2002), and seizures (Choi et al. 2003a, b; Rosell et al. 2003). Whether increases in gp130-associated STAT3 expression after such a variety of perturbations contribute to subsequent cell death or survival is not fully understood. Numerous studies demonstrate that IL-6 exerts multiple effects, both beneficial and destructive, on CNS cells. In glial cells, IL-6 promotes astrocyte proliferation and is believed to be involved in astrogliosis (Van Wagoner and Benveniste 1999). The present study provided evidence that the mouse gp130 antibody suppressed the PGE_2 formation induced by IL-6 as well as IL-6/sIL-6R complexes in a dose-dependent manner (Fig. 5), suggesting that the IL-6/sIL-6R/gp130 system can modulate the function of PGE_2 synthesis in astrocytes.

Although the precise mechanism underlying induction of PGE_2 synthesis by IL-6 has not yet been elucidated, IL-6/sIL-6R and the signal transducer gp130 play important roles in the regulation of COX-2 expression and subsequent PGE_2 formation in mouse astrocytes, and IL-6 is an important regulator of immune and inflammatory processes in the CNS.

Acknowledgments We are very grateful to Dr. Akira Tanaka for his valuable and helpful advice on the experiments and manuscript preparation.

References

Almer, G., Guegan, C., Teismann, P., et al. (2001). Increased expression of the pro-inflammatory enzyme cyclooxygenase-2 in amyotrophic lateral sclerosis. *Annals of Neurology, 49*, 176–185. doi:10.1002/1531-8249(20010201)49:2<176::AID-ANA37>3.0.CO;2-X.

Bauer, M. K. A., Lieb, K., Schulze-Osthoff, K., et al. (1997). Expression and regulation of cyclooxygenase-2 in rat microglia. *European Journal of Biochemistry, 243*, 726–731. doi:10.1111/j.1432-1033.1997.00726.x.

Bezzi, P., Carmignoto, G., Pasti, L., et al. (1998). Prostaglandins stimulate calcium-dependent glutamate release in astrocytes. *Nature, 391*, 281–285. doi:10.1038/34651.

Bishai, I., & Coceani, F. (1992). Eicosanoid formation in the rat cerebral cortex. *Molecular and Chemical Neuropathology, 17*, 219–238.

Bradford, M. M. (1976). A rapid and sensitive method for the quantitation of microgram quantities of protein utilizing the principle of protein-dye binding. *Analytical Biochemistry, 72*, 248–254. doi:10.1016/0003-2697(76)90527-3.

Choi, J. -S., Kim, S. Y., Cha, J. -H., et al. (2003a). Upregulation of gp130 and STAT3 activation in the rat hippocampus following

transient forebrain ischemia. *Glia, 41*, 237–246. doi:10.1002/glia.10186.

Choi, J. -S., Kim, S. Y., Park, H. -J., et al. (2003b). Upregulation of gp130 and differential activation of STAT and p42/44 MAPK in the rat hippocampus following kainic acid-induced seizures. *Brain Research. Molecular Brain Research, 119*, 10–18. doi:10.1016/j.molbrainres.2003.08.010.

Dayton, E. T., & Major, E. O. (1996). Recombinant human interleukin 1β induces production of prostaglandins in primary human fetal astrocytes and immortalized human fetal astrocyte cultures. *Journal of Neuroimmunology, 71*, 11–18. doi:10.1016/S0165-5728(96)00111-7.

DeWitt, D. L., & Smith, W. L. (1988). Primary structure of prostaglandin G/H synthase from sheep vesicular gland determined from the complementary DNA sequence. *Proceedings of the National Academy of Sciences of the United States of America, 85*, 1412–1416. doi:10.1073/pnas.85.5.1412.

Drachman, D. B., & Rothstein, J. D. (2000). Inhibition of cyclooxygenase-2 protects motor neurons in an organotypic model of amyotrophic lateral sclerosis. *Annals of Neurology, 48*, 792–795. doi:10.1002/1531-8249(200011)48:5<792::AID-ANA14>3.0.CO;2-5.

Dubois, R. N., Abramson, S. B., Crofford, L., et al. (1998). Cyclooxygenase in biology and disease. *The FASEB Journal, 12*, 1063–1073.

Fontana, A., Kristensen, F., Dubs, R., Gemsa, D., & Weber, E. (1982). Production of prostaglandin E and an interleukin-1 like factor by cultured astrocytes and C_6 glioma cells. *Journal of Immunology (Baltimore, MD.: 1950), 129*, 2413–2419.

Gadient, R. A., & Otten, U. (1994). Identification of interleukin-6(IL-6)-expressing neurons in the cerebellum and hippocampus of normal adult rats. *Neuroscience Letters, 182*, 243–246. doi:10.1016/0304-3940(94)90807-9.

Gautron, L., Lafon, P., Chaigniau, M., Tramu, G., & Laye, S. (2002). Spatiotemporal analysis of signal transducer and activator of transcription 3 activation in rat brain astrocytes and pituitary following peripheral immune challenge. *Neuroscience, 112*, 717–729. doi:10.1016/S0306-4522(02)00115-X.

Hayaishi, O. (1991). Molecular mechanisms of sleep-wake regulation: Roles of prostaglandins D_2 and E_2. *The FASEB Journal, 5*, 2575–2581.

Heinrich, P. C., Behrmann, I., Muller-Newen, G., Schaper, F., & Graeve, L. (1998). Interleukin-6-type cytokine signalling through the gp130/Jak/STAT pathway. *The Biochemical Journal, 334*, 297–314.

Hibi, M., Murakami, M., Saito, M., Hirano, T., Taga, T., & Kishimoto, T. (1990). Molecular cloning and expression of an IL-6 signal transducer, gp130. *Cell, 63*, 1149–1157. doi:10.1016/0092-8674(90)90411-7.

Ishimoto, H., Nakahata, N., Matsuoka, I., & Nakanishi, H. (1997). Effects of ATP on phosphoinositide hydrolysis and prostaglandin E_2 generation in rabbit astrocytes. *The Journal of Pharmacy and Pharmacology, 49*, 520–524.

Jacobs, T. P., Shohami, E., Baze, W., et al. (1987). Deteriorating stroke model: Histopathology, edema, and eicosanoid changes following spinal cord ischemia in rabbits. *Stroke, 18*, 741–750.

Justicia, C., Gabriel, C., & Planas, A. M. (2000). Activation of the JAK/STAT pathway following transient focal cerebral ischemia: Signaling through Jak1 and Stat3 in astrocytes. *Glia, 30*, 253–270. doi:10.1002/(SICI)1098-1136(200005)30:3<253::AID-GLIA5>3.0.CO;2-O.

Kaartinen, V., Voncken, J. W., Shuler, C., et al. (1995). Abnormal lung development and cleft palate in mice lacking TGF-β3 indicates defects of epithelial-mesenchymal interaction. *Nature Genetics, 11*, 415–421. doi:10.1038/ng1295-415.

Kishimoto, T., Taga, T., & Akira, S. (1994). Cytokine signal transduction. *Cell, 76*, 253–262. doi:10.1016/0092-8674(94)90333-6.

Kordula, T., Rydel, R. E., Brigham, E. F., Horn, F., Heinrich, P. C., & Travis, J. (1998). Oncostatin M and the interleukin-6 and soluble interleukin-6 receptor complex regulate α_1-antichymotrypsin expression in human cortical astrocytes. *The Journal of Biological Chemistry, 273*, 4112–4118. doi:10.1074/jbc.273.7.4112.

Kudo, I., & Murakami, M. (1999). Diverse functional coupling of prostanoid biosynthetic enzymes in various cell types. *Advances in Experimental Medicine and Biology, 469*, 29–35.

Lin, A. H., Bienkowski, M. J., & Gorman, R. R. (1989). Regulation of prostaglandin H synthase mRNA levels and prostaglandin biosynthesis by platelet-derived growth factor. *The Journal of Biological Chemistry, 264*, 17379–17383.

Liu, X. -H., Kirschenbaum, A., Lu, M., et al. (2002). Prostaglandin E_2 stimulates prostatic intraepithelial neoplasia cell growth through activation of the interleukin-6/gp130/Stat-3 signaling pathway. *Biochemical and Biophysical Research Communications, 290*, 249–255. doi:10.1006/bbrc.2001.6188.

Luo, J., Lang, J. A., & Miller, M. W. (1998). Transforming growth factor β1 regulates the expression of cyclooxygenase in cultured cortical astrocytes and neurons. *Journal of Neurochemistry, 71*, 526–534.

Lust, J. A., Donovan, K. A., Kline, M. P., Greipp, P. R., Kyle, R. A., & Maihle, N. J. (1992). Isolation of an mRNA encoding a soluble form of the human interleukin-6 receptor. *Cytokine, 4*, 96–100. doi:10.1016/1043-4666(92)90043-Q.

Marcheselli, V. L., & Bazan, N. G. (1996). Sustained induction of prostaglandin endoperoxide synthetase-2 by seizures in hippocampus. *The Journal of Biological Chemistry, 271*, 24794–24799. doi:10.1074/jbc.271.40.24794.

Marz, P., Cheng, J. G., Gadient, R. A., et al. (1998). Sympathetic neurons can produce and respond to interleukin 6. *Proceedings of the National Academy of Sciences of the United States of America, 95*, 3251–3256. doi:10.1073/pnas.95.6.3251.

McGeer, P. L., McGeer, E., Rogers, J., & Sibley, J. (1990). Anti-inflammatory drugs and Alzheimer disease. *Lancet, 335*, 1037. doi:10.1016/0140-6736(90)91101-F.

Minghetti, L., & Levi, G. (1995). Induction of prostanoid biosynthesis by bacterial lipopolysaccharide and isoproterenol in rat microglial cultures. *Journal of Neurochemistry, 65*, 2690–2698.

Minghetti, L., Walsh, D. T., Levi, G., & Perry, V. H. (1999). In vivo expression of cyclooxygenase-2 in rat brain following intraparenchymal injection of bacterial endotoxin and inflammatory cytokines. *Journal of Neuropathology and Experimental Neurology, 58*, 1184–1191. doi:10.1097/00005072-199911000-00008.

Molina-Holgado, E., Ortiz, S., Molina-Holgado, F., & Guaza, C. (2000). Induction of COX-2 and PGE_2 biosynthesis by IL-1β is mediated by PKC and mitogen-activated protein kinases in murine astrocytes. *British Journal of Pharmacology, 131*, 152–159. doi:10.1038/sj.bjp.0703557.

Mollace, V., Colasanti, M., Muscoli, C., et al. (1998). The effect of nitric oxide on cytokine-induced release of PGE_2 by human cultured astroglial cells. *British Journal of Pharmacology, 124*, 742–746. doi:10.1038/sj.bjp.0701852.

Montine, T. J., Sidell, K. R., Crews, B. C., et al. (1999). Elevated CSF prostaglandin E_2 levels in patients with probable AD. *Neurology, 53*, 1495–1498.

Morham, S. G., Langenbach, R., Loftin, C. D., et al. (1995). Prostaglandin synthase 2 gene disruption causes severe renal pathology in the mouse. *Cell, 83*, 473–482. doi:10.1016/0092-8674(95)90125-6.

Mullberg, J., Schooltink, H., Stoyan, T., et al. (1993). The soluble interleukin-6 receptor is generated by shedding. *European Journal of Immunology, 23*, 473–480. doi:10.1002/eji.1830230226.

Mullberg, J., Oberthur, W., Lottspeich, F., et al. (1994). The soluble human IL-6 receptor: Mutational characterization of the proteo-

lytic cleavage site. *Journal of Immunology (Baltimore, MD.: 1950), 152*, 4958–4968.

Nogawa, S., Zhang, F., Ross, M. E., & Iadecola, C. (1997). Cyclo-oxygenase-2 gene expression in neurons contributes to ischemic brain damage. *The Journal of Neuroscience, 17*, 2746–2755.

O'Banion, M. K., Winn, V. D., & Young, D. A. (1992). cDNA cloning and functional activity of a glucocorticoid-regulated inflammatory cyclooxygenase. *Proceedings of the National Academy of Sciences of the United States of America, 89*, 4888–4892. doi:10.1073/pnas.89.11.4888.

O'Banion, M. K., Miller, J. C., Chang, J. W., Kaplan, M. D., & Coleman, P. D. (1996). Interleukin-1β induces prostaglandin G/H synthase-2 (cyclooxygenase-2) in primary murine astrocyte cultures. *Journal of Neurochemistry, 66*, 2532–2540.

Oh, J. -W., Wagoner, N. J. V., Rose-John, S., & Benveniste, E. N. (1998). Role of IL-6 and the soluble IL-6 receptor in inhibition of VCAM-1 gene expression. *Journal of Immunology (Baltimore, MD.: 1950), 161*, 4992–4999.

Pasti, L., Zonta, M., Pozzan, T., Vicini, S., & Carmignoto, G. (2001). Cytosolic calcium oscillations in astrocytes may regulate exocytotic release of glutamate. *The Journal of Neuroscience, 21*, 477–484.

Peters, M., Muller, A. M., & Rose-John, S. (1998). Interleukin-6 and soluble interleukin-6 receptor: direct stimulation of gp130 and hematopoiesis. *Blood, 92*, 3495–3504.

Pilbeam, C. C., Kawaguchi, H., Hakeda, Y., Voznesensky, O., Alander, C. B., & Raisz, L. G. (1993). Differential regulation of inducible and constitutive prostaglandin endoperoxide synthase in osteoblastic MC3T3-E1 cells. *The Journal of Biological Chemistry, 268*, 25643–25649.

Pistritto, G., Mancuso, C., Tringali, G., Perretti, M., Preziosi, P., & Navarra, P. (1998). The relative contribution of constitutive and inducible cyclooxygenase activity to lipopolysaccharide-induced prostaglandin production by primary cultures of rat hypothalamic astrocytes. *Neuroscience Letters, 246*, 45–48. doi:10.1016/S0304-3940(98)00226-2.

Pistritto, G., Franzese, O., Pozzoli, G., et al. (1999). Bacterial lipopolysaccharide increases prostaglandin production by rat astrocytes via inducible cyclo-oxygenase: Evidence for the involvement of nuclear factor κB. *Biochemical and Biophysical Research Communications, 263*, 570–574. doi:10.1006/bbrc.1999.1413.

Pritchard, K. A., O'Banion, M. K., Miano, J. M., et al. (1994). Induction of cyclooxygenase-2 in rat vascular smooth muscle cells in vitro and in vivo. *The Journal of Biological Chemistry, 269*, 8504–8509.

Repovic, P., Mi, K., & Benveniste, E. N. (2003). Oncostatin M enhances the expression of prostaglandin E_2 and cyclooxygenase-2 in astrocytes: Synergy with interleukin-1β, tumor necrosis factor-α, and bacterial lipopolysaccharide. *Glia, 42*, 433–446. doi:10.1002/glia.10182.

Rose-John, S., & Heinrich, P. C. (1994). Soluble receptors for cytokines and growth factors: generation and biological function. *The Biochemical Journal, 300*, 281–290.

Rosell, D. R., Akama, K. T., Nacher, J., & McEwen, B. S. (2003). Differential expression of suppressors of cytokine signaling-1, -2, and -3 in the rat hippocampus after seizure: Implications for neuromodulation by gp130 cytokines. *Neuroscience, 122*, 349–358. doi:10.1016/S0306-4522(03)00594-3.

Saas, P., Boucraut, J., Walker, P. R., et al. (2000). TWEAK stimulation of astrocytes and the proinflammatory consequences. *Glia, 32*, 102–107. doi:10.1002/1098-1136(200010)32:1<102::AID-GLIA100>3.0.CO;2-U.

Samad, T. A., Moore, K. A., Sapirstein, A., et al. (2001). Interleukin 1β-mediated induction of cox-2 in the CNS contributes to inflammatory pain hypersensitivity. *Nature, 410*, 471–475. doi:10.1038/35068566.

Sawada, M., Suzumura, A., Ohno, K., & Marunouchi, T. (1993). Regulation of astrocyte proliferation by prostaglandin E_2 and the α subtype of protein kinase C. *Brain Research, 613*, 67–73. doi:10.1016/0006-8993(93)90455-V.

Sawada, M., Suzumura, A., & Marunouchi, T. (1995). Cytokine network in the central nervous system and its roles in growth and differentiation of glial and neuronal cells. *International Journal of Developmental Neuroscience, 13*, 253–264. doi:10.1016/0736-5748(94)00076-F.

Seregi, A., Keller, M., Jackisch, R., & Hertting, G. (1984). Comparison of the prostanoid synthesizing capacity in homogenates from primary neuronal and astroglial cell cultures. *Biochemical Pharmacology, 33*, 3315–3318. doi:10.1016/0006-2952(84)90099-6.

Smith, W. L., Garavito, R. M., & DeWitt, D. L. (1996). Prostaglandin endoperoxide H synthases(cyclooxygenases)-1 and -2. *The Journal of Biological Chemistry, 271*, 33157–33160. doi:10.1074/jbc.271.52.33157.

Smith, W. L., DeWitt, D. L., & Garavito, R. M. (2000). Cyclooxygenases: Structural, cellular, and molecular biology. *Annual Review of Biochemistry, 69*, 145–182. doi:10.1146/annurev.biochem.69.1.145.

Stephenson, D. T., Lemere, C. A., Selkoe, D. J., & Clemens, J. A. (1996). Cytosolic phospholipase A_2(cPLA$_2$) immunoreactivity is elevated in Alzheimer's disease brain. *Neurobiology of Disease, 3*, 51–63. doi:10.1006/nbdi.1996.0005.

Taga, T., & Kishimoto, T. (1997). Gp130 and the interleukin-6 family of cytokines. *Annual Review of Immunology, 15*, 797–819. doi:10.1146/annurev.immunol.15.1.797.

Teather, L. A., Lee, R. K. K., & Wurtman, R. J. (2002). Platelet-activating factor increases prostaglandin E_2 release from astrocyte-enriched cortical cell cultures. *Brain Research, 946*, 87–95. doi:10.1016/S0006-8993(02)02866-4.

Their, M., Marz, P., Otten, U., Weis, J., & Rose-John, S. (1999). Interleukin-6(IL-6) and its soluble receptor support survival of sensory neurons. *Journal of Neuroscience Research, 55*, 411–422. doi:10.1002/(SICI)1097-4547(19990215)55:4<411::AID-JNR2>3.0.CO;2-D.

Ushikubi, F., Segi, E., Sugimoto, Y., et al. (1998). Impaired febrile response in mice lacking the prostaglandin E receptor subtype EP_3. *Nature, 395*, 281–284. doi:10.1038/26233.

Van Wagoner, N. J., & Benveniste, E. N. (1999). Interleukin-6 expression and regulation in astrocytes. *Journal of Neuroimmunology, 100*, 124–139. doi:10.1016/S0165-5728(99)00187-3.

Vane, J. R., Bakhle, Y. S., & Botting, R. M. (1998). Cyclooxygenases 1 and 2. *Annual Review of Pharmacology and Toxicology, 38*, 97–120. doi:10.1146/annurev.pharmtox.38.1.97.

Xie, W., Chipman, J. G., Robertson, D. L., Erikson, R. L., & Simmons, D. L. (1991). Expression of a mitogen-responsive gene encoding prostaglandin synthase is regulated by mRNA splicing. *Proceedings of the National Academy of Sciences of the United States of America, 88*, 2692–2696. doi:10.1073/pnas.88.7.2692.

Xu, J., Chalimoniuk, M., Shu, Y., et al. (2003). Prostaglandin E_2 production in astrocytes: Regulation by cytokines, extracellular ATP, and oxidative agents. *Prostaglandins, Leukotrienes, and Essential Fatty Acids, 69*, 437–448. doi:10.1016/j.plefa.2003.08.016.

Yamagata, K., Andreasson, K. I., Kaufmann, W. E., Barnes, C. A., & Worley, P. F. (1993). Expression of a mitogen-inducible cyclooxygenase in brain neurons: Regulation by synaptic activity and glucocorticoids. *Neuron, 11*, 371–386.